CONCRETE LIBRARY OF JSCE NO. 29, JUNE 1997

DEVELOPMENT AND VERIFICATION OF ENHANCED MICROPLANE CONCRETE MODEL

(Summarized translation from Proceedings of JSCE, No.538/V-31, May 1996)

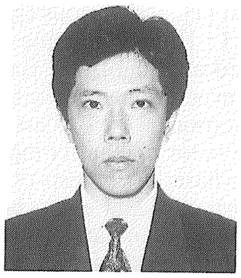

Toshiaki HASEGAWA

The difference between the normal-shear and volumetric-deviatoric-shear component formulations, on which microplane models by Hasegawa and Prat are respectively based, is examined by numerical analysis for a wide range of stress conditions. Then the Hasegawa model (Microplane Concrete Model) is improved to expand its applicability and reformulated as the Enhanced Microplane Concrete Model serving as a more general constitutive law. One of the major improvements is to take into account the resolved lateral stress in normal compression response on a microplane as well as the resolved lateral strain. Another major improvement is to adopt a model for the transition from brittle to ductile fracture for the shear response on a microplane at increasing resolved normal compression stress. It is verified that the Enhanced Microplane Concrete Model can predict well the experimentally obtained constitutive relations for concrete reported in the literature, covering various stress conditions and cyclic loading. Examination of the microplane responses in each analysis explains the load-carrying mechanisms in concrete in terms of the responses on the microplanes.

Key Words : *general constitutive law, multiaxial stress, biaxial stress, cyclic response, applicability to concrete*

Toshiaki HASEGAWA is a structural research engineer at Shimizu Corporation, Tokyo, Japan. He received both his Bachelor's and Master's degrees in civil engineering from Waseda University, Tokyo and Doctor of Engineering degree from the University of Tokyo. His research interests include not only the constitutive relations and fracture of concrete but also creep and shrinkage of concrete.

---

1. INTRODUCTION

Since the accuracy of finite element analysis for concrete structures depends on the constitutive model (stress-strain relation) of the concrete, which describes cracking, damage, plasticity, etc., various constitutive laws dealing with the complicated nonlinearity of concrete have been developed. The microplane model is one of such constitutive laws. It has a clear physical image at the microscopic level, and is based on a characteristic hypothesis that the inelastic origin of concrete as a heterogeneous material is microcracks which occur within the interface region (microplane) between the coarse aggregate particle and the mortar matrix.

The model was first proposed by Bazant [1], and various types of the model have been developed by he and his co-workers as shown in **Fig.1**. However, some of the models sacrifice the conceptional clearness of the microplane to expanded applicability. Bazant and Gambarova [2] developed the normal component formulation in which an additional elastic body was incorporated with the microplane system to adjust Poisson's ratio. Recent models by Bazant and Prat [3], Ozbolt and Bazant [4], and Carol et al. [5] adopted a volumetric-deviatoric-shear component formulation to obtain an arbitrary Poisson's ratio. It seems to go against the basic hypothesis of the microplane model to split microplane responses into an overall macroscopic response and individual microplane responses. In view of the previous microplane models losing conceptual clearness, Hasegawa and Bazant [6] developed the Microplane Concrete Model based on a normal-shear component formulation in which no additional elastic body or volumetric component of microplane is used to adjust Poisson's ratio.

In this study [7] the Microplane Concrete Model, based on the fundamental idea of the microplane, is pursued with accuracy so that it can be used as a practical constitutive law. The prediction limitations of this model as well as those of a previous model are clarified through various analyses. Then the model is reformulated as the Enhanced Microplane Concrete Model to provide a model that is reasonably sophisticated and more accurate while offering wider applicability. The model is verified by comparing the analytical results with experimental data from the literature. The load-carrying mechanisms of concrete are discussed through comparison between constitutive relations (macroscopic behavior) obtained by the model and the responses on microplanes (microscopic behavior).

2. GENERAL APPLICABILITY OF MICROPLANE MODELS TO CONCRETE

Among the previous models shown in **Fig.1**, only the models based on a volumetric-deviatoric-shear component formulation (Prat model, Ozbolt model, and Carol model) and the Hasegawa model (Microplane Concrete Model) based on a normal-shear component formulation are applicable to general multiaxial stress conditions. In this first part of the present study, the prediction accuracy of both formulations for general multiaxial stress conditions are examined by comparing the calculated results they yield.

Since the Hasegawa model and the Prat model are different not only in basic formulation but also in their definitions of shear strain on microplane and the constitutive relations of the microplane (microconstitutive relations), it is not appropriate to directly compare results obtained by the two models. In this study attention is focused on the difference in the basic formulations of the models, and the characteristics of these formulations are clarified. For that purpose, the Hasegawa model with the normal-shear component formulation is compared with a modified model in which the basic formulation is substituted by the volumetric-deviatoric-shear component formulation.

2.1 The Hasegawa Model (Normal-Shear Component Formulation)

In the Hasegawa model the incremental forms of the microconstitutive relations are written separately for the normal component and the shear components in the K and M directions

normal component: $d\sigma_N = C_N d\varepsilon_N - d\sigma_N''$ (1a)

K-shear component: $d\sigma_{TK} = C_{TK} d\varepsilon_{TK} - d\sigma_{TK}''$ (1b)

M-shear component: $d\sigma_{TM} = C_{TM} d\varepsilon_{TM} - d\sigma_{TM}''$ (1c)

- static constraint type
  - Prat model (creep model for anisotropic clay)
- kinematic constraint type
  - normal component formulation
    - Gambarova model, Oh model
  - normal-shear component formulation
    - Kim model
  - volumetric-deviatoric-shear component formulation
    - Carol model
- mixed kinematic-static constraint type
  - volumetric-deviatoric-shear component formulation
    - Prat model, Ozbolt model
  - normal-shear component formulation
    - Hasegawa model

Fig.1 Various types of microplane model

in which $d\sigma_N$, $d\sigma_{TK}$, and $d\sigma_{TM}$ = microplane stress increments; C_N, C_{TK}, and C_{TM} = incremental elastic stiffnesses for the microplane; and $d\sigma_N''$, $d\sigma_{TK}''$, and $d\sigma_{TM}''$ = inelastic microplane stress increments.

The incremental form of the macroscopic constitutive relation for the Hasegawa model is written as (2).

$$d\sigma_{ij} = C_{ijrs} d\varepsilon_{rs} - d\sigma_{ij}'' \tag{2a}$$

$$C_{ijrs} = \frac{3}{2\pi}\int_S \Big[n_i n_j n_r n_s C_N + \frac{1}{4}(k_i n_j + k_j n_i)(k_r n_s + k_s n_r) C_{TK} + \frac{1}{4}(m_i n_j + m_j n_i)(m_r n_s + m_s n_r) C_{TM} \Big] f(\mathbf{n}) dS \tag{2b}$$

$$d\sigma_{ij}'' = \frac{3}{2\pi}\int_S \Big[n_i n_j d\sigma_N'' + \frac{1}{2}(k_i n_j + k_j n_i) d\sigma_{TK}'' + \frac{1}{2}(m_i n_j + m_j n_i) d\sigma_{TM}'' \Big] f(\mathbf{n}) dS \tag{2c}$$

in which C_{ijrs} = the incremental elastic stiffness tensor; $d\sigma_{ij}''$ = inelastic stress increment; S = surface of unit hemisphere; n_i or $\mathbf{n}$ = the normal unit vector of microplane; k_i and m_i = in-plane unit coordinate vectors normal to each other on microplane; and $f(\mathbf{n})$ = a weight function for the normal direction $\mathbf{n}$. In this paper, indicial notation is used for tensors and the Latin lower-case subscripts refer to Cartesian coordinates x_i, $i = 1, 2, 3$ (x, y, z).

The derivation of (2) is shown later. The formulation of individual microconstitutive relation is well described in [6].

2.2 Volumetric-Deviatoric-Shear Component Formulation

In the volumetric-deviatoric-shear component formulation considered here, normal strains ε_N in the normal-shear component formulation are decomposed into a volumetric strain $\varepsilon_V = \varepsilon_{kk}/3$ and deviatoric strains $\varepsilon_D = \varepsilon_N - \varepsilon_V$ which are different for each microplane, and a volumetric stress σ_V corresponding to the volumetric strain ε_V and deviatoric stresses σ_D corresponding to the deviatoric strains ε_D on the microplanes are calculated.

The incremental form (1a) of the microconstitutive relation for the normal component is replaced by incremental forms for volumetric and deviatoric components ((3a) and (3b))

$$\text{volumetric component: } d\sigma_V = C_V d\varepsilon_V - d\sigma_V'' \tag{3a}$$

$$\text{deviatoric component: } d\sigma_D = C_D d\varepsilon_D - d\sigma_D'' \tag{3b}$$

in which $d\sigma_V$, C_V, and $d\sigma_V''$ = microplane stress increment, incremental elastic stiffness, and inelastic microplane stress increment for the volumetric component; and $d\sigma_D$, C_D, and $d\sigma_D''$ = microplane stress increment, incremental elastic stiffness, and inelastic microplane stress increment for the deviatoric component.

Table 1 Material parameters for normal-shear component formulation

normal tension	σ^0_{NT} (kgf/cm^2)	40.0
	ζ_{NT}	0.5
	γ_{NT}	5.0
	p_{NT}	1.0
	ρ_{NT} (sec)	10^5
normal compression (softening)	σ^0_{NC} (kgf/cm^2)	-400
	ζ_{NC}	0.3
	γ_{NC}	1.0
	p_{NC}	1.0
	ρ_{NC} (sec)	10^7
shear	σ^0_T (kgf/cm^2)	17.0
	ζ_T	0.5
	γ_T	1.5
	p_T	1.0
	μ	0.6
	ρ_T (sec)	10^6
lateral strain effect	ε^1_{LD}	0.01
	ε^p_{LD}	0.01
	m	1.0

Table 2 Material parameters for volumetric-deviatoric-shear component formulation

deviatoric tension	σ^0_{DT} (kgf/cm^2)	25.0
	ζ_{DT}	0.5
	γ_{DT}	5.0
	p_{DT}	1.0
	ρ_{DT} (sec)	10^5
deviatoric compression	σ^0_{DC} (kgf/cm^2)	-200
	ζ_{DC}	0.5
	γ_{DC}	2.0
	p_{DC}	1.0
	ρ_{DC} (sec)	10^6
shear	σ^0_T (kgf/cm^2)	60.0
	ζ_T	0.5
	γ_T	2.0
	p_T	1.0
	μ	0.7
	ρ_T (sec)	10^6
volumetric tension	σ^0_{VT} (kgf/cm^2)	25.0
	ζ_{VT}	0.5
	γ_{VT}	5.0
	p_{VT}	1.0
	ρ_{VT} (sec)	10^5
$\eta_0 = C^0_D / C^0_V$		1.0

The incremental form of the macroscopic constitutive relation of the volumetric-deviatoric-shear component formulation is written as (4).

$$d\sigma_{ij} = C_{ijrs} d\varepsilon_{rs} - d\sigma_{ij}'' \tag{4a}$$

$$C_{ijrs} = \frac{3}{2\pi}\int_S \left[\frac{1}{3} n_i n_j \delta_{rs} C_V + n_i n_j \left(n_r n_s - \frac{1}{3}\delta_{rs} \right) C_D + \frac{1}{4}\left(k_i n_j + k_j n_i\right)\left(k_r n_s + k_s n_r\right) C_{TK} + \frac{1}{4}\left(m_i n_j + m_j n_i\right)\left(m_r n_s + m_s n_r\right) C_{TM} \right] f(\mathbf{n}) dS \tag{4b}$$

$$d\sigma_{ij}'' = \frac{3}{2\pi}\int_S \left[n_i n_j \left(d\sigma_V'' + d\sigma_D''\right) + \frac{1}{2}\left(k_i n_j + k_j n_i\right) d\sigma_{TK}'' + \frac{1}{2}\left(m_i n_j + m_j n_i\right) d\sigma_{TM}'' \right] f(\mathbf{n}) dS \tag{4c}$$

in which δ_{rs} = Kronecker's unit delta tensor.

In the volumetric-deviatoric-shear component formulation a lateral strain dependence of normal microplane response is indirectly taken into account by resolving the normal microplane response into volumetric and deviatoric responses. The volumetric loading curve in the volumetric-deviatoric-shear component formulation is identical to the hydrostatic loading curve of the normal component in the normal-shear component formulation.

2.3 Comparative Analysis

To compare the normal-shear and volumetric-deviatoric-shear component formulations, a series of numerical analyses is done using both over a wider range of stress conditions.

Triaxial compressive tests along the compressive meridian carried out by Smith et al. [8] are first simulated using both formulations, and then triaxial compressive analysis along the tensile meridian, biaxial compression analysis, biaxial compression-tension analysis, and biaxial tension analysis are done with identical input material parameters to simulate the tests by Smith et al. The material parameters for the analyses are shown in **Tables 1** and **2** for the normal-shear and volumetric-deviatoric-shear component formulations, respectively. The definitions of the parameters are given in Hasegawa's study [6], and other parameters not shown in the tables are the same as those used in that study.

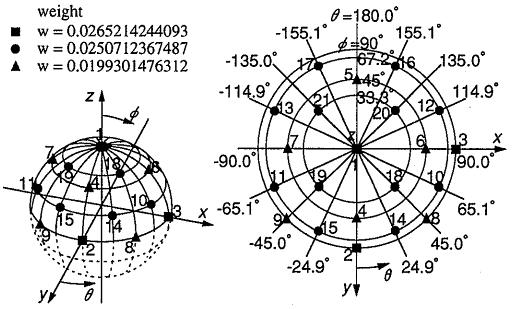

Fig.2 Numerical integration points on unit hemisphere

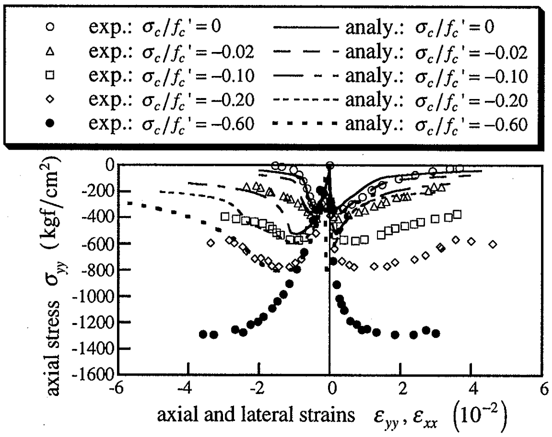

(a) Normal-shear component formulation

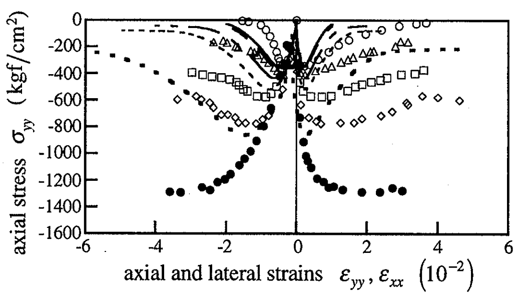

(b) Volumetric-deviatoric-shear component formulation

Fig.3 Triaxial compression analysis along compressive meridian

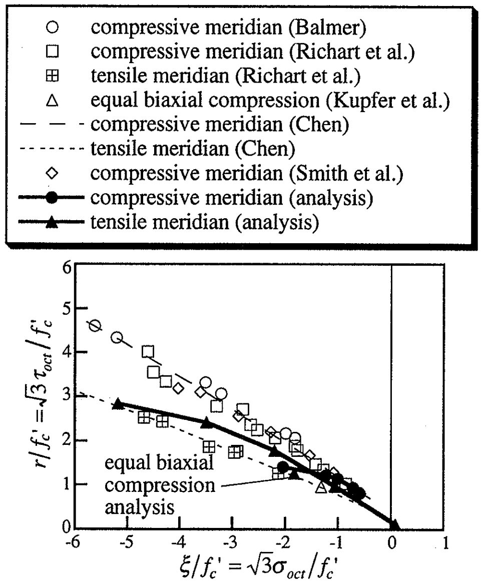

(a) Normal-shear component formulation

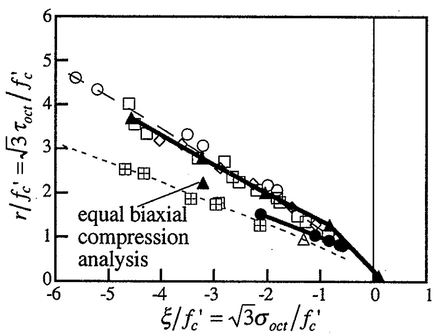

(b) Volumetric-deviatoric-shear component formulation

Fig.4 Compressive and tensile meridians

The integrations in (2) and (4) are evaluated using the numerical integration formula derived by Bazant and Oh [9]. The integration points and weights for the formula are shown in **Fig.2**.

a) Triaxial Compression Analysis

In **Fig.3** the triaxial compressive responses from the analysis are compared with the test results of Smith et al., in which σ_c is confinement pressure and f_c' is uniaxial compressive strength. Neither the normal-shear component formulation nor the volumetric-deviatoric-shear component formulation can predict confinement effect and the transition from brittle to ductile fracture well. The compressive and tensile meridians of the failure envelope are evaluated from maximum stresses obtained in the

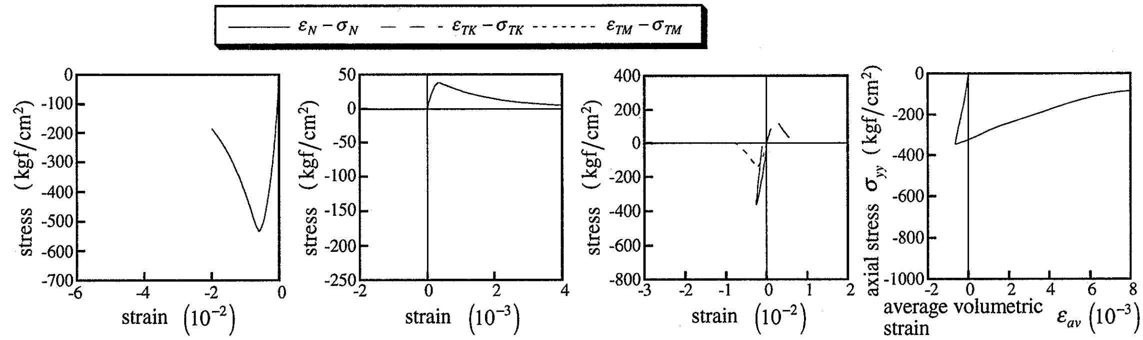

(a) Microplane 2 (b) Microplane 3 (c) Microplane 14 (d) Average volumetric response

Fig.5 Responses in uniaxial compression analysis using normal-shear component formulation

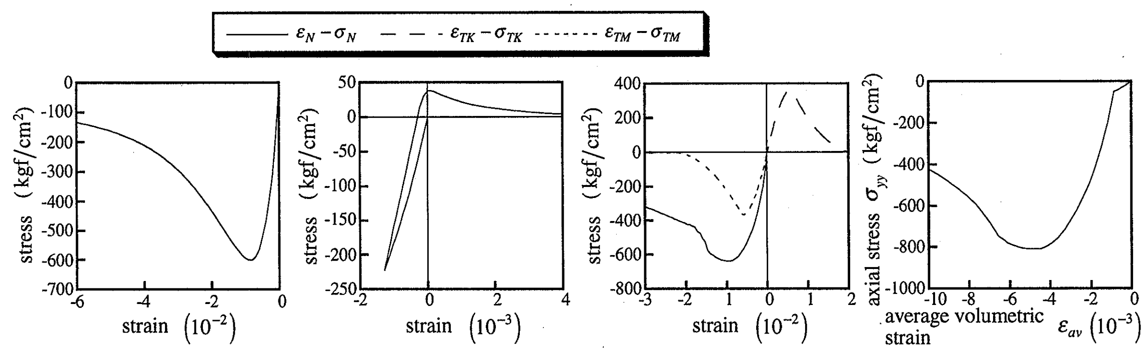

(a) Microplane 2 (b) Microplane 3 (c) Microplane 14 (d) Average volumetric response

Fig.6 Responses in triaxial compression analysis $(\sigma_c/f_c' = -0.60)$ using normal-shear component formulation

analyses, and shown in **Fig.4** with experimental results from the literature (Balmer [10], Richart et al. [11], Kupfer et al. [12], Smith et al. [8], and Chen [13]), where $\sigma_{oct} = I_1/3 = \sigma_{ii}/3$ and $\tau_{oct} = \sqrt{2J_2/3}$ are octahedral normal and shear stresses (J_2 = the 2nd invariant of deviatoric stress tensor). In the case of the normal-shear component formulation, the compressive meridian under low confinement stress agrees well with the experimental data; however, it deviates from the experimental data under higher confinement stress and tends to approach the σ_{oct} axis. On the other hand, in the case of the volumetric-deviatoric-shear component formulation the tensile meridian is above the compressive one in contrast with the experimental results.

Figs.5 and **6** show the normal, K-shear, and M-shear responses of microplanes (integration points) 2, 3, and 14 as well as the average volumetric responses ε_{av} for the uniaxial $(\sigma_c/f_c' = 0)$ and triaxial $(\sigma_c/f_c' = -0.60)$ compression analyses using the normal-shear component formulation $(\varepsilon_{av} = \varepsilon_{ii}/3)$. It is obvious from **Fig.5(b)** that normal tension damage of microplane 3, representing splitting cracks under lower macroscopic compressive stress, results in lower macroscopic strength in the uniaxial compression analysis. On the other hand, normal compression stress occurring on microplane 3 when macroscopic confinement pressure is applied delays normal tension damage of the microplane as if it were a prestress, resulting in higher macroscopic strength in the triaxial compression analysis (**Fig.6(b)**). Since all microplanes ultimately exhibit strain-softening responses, as shown in **Figs.6(a)** - **(c)**, increases in macroscopic strength and ductility with confinement pressure cannot be predicted well by the normal-shear component formulation.

Figs.7 and **8** show the deviatoric, K-shear, and M-shear responses of microplanes (integration points)

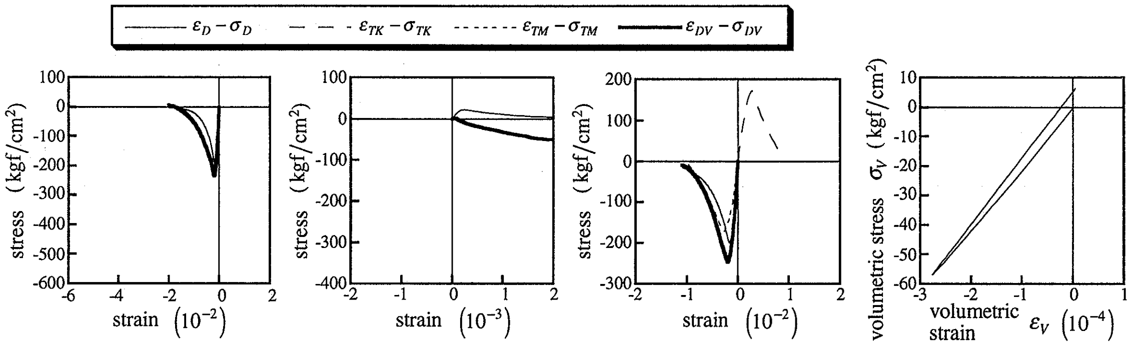

(a) Microplane 2 (b) Microplane 3 (c) Microplane 14 (d) Volumetric response

Fig.7 Responses in uniaxial compression analysis using volumetric-deviatoric-shear component formulation

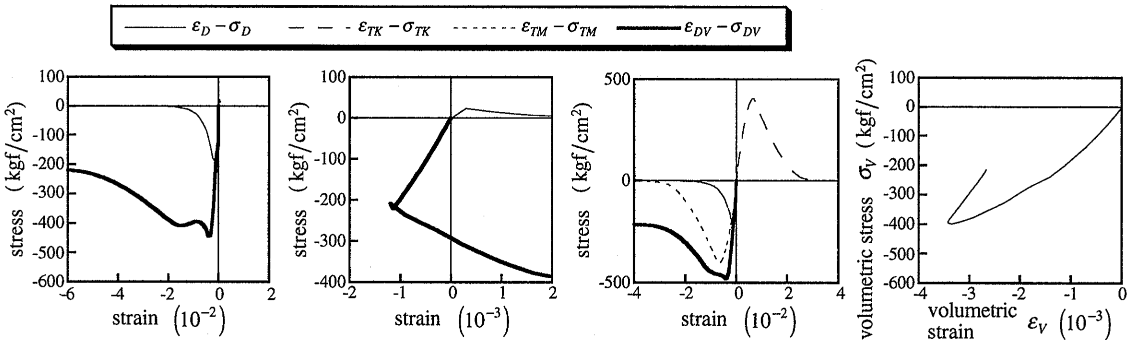

(a) Microplane 2 (b) Microplane 3 (c) Microplane 14 (d) Volumetric response

Fig.8 Responses in triaxial compression analysis $(\sigma_c/f_c' = -0.60)$ using volumetric-deviatoric-shear component formulation

2, 3, and 14 as well as the volumetric responses for the uniaxial $(\sigma_c/f_c' = 0)$ and triaxial $(\sigma_c/f_c' = -0.60)$ compression analyses using the volumetric-deviatoric-shear component formulation. The total normal responses (ε_{DV}-σ_{DV} relations) as sums of the deviatoric and volumetric components are also shown in **Figs.7(a) - (c)** and **Figs.8(a) - (c)**. The difference between the deviatoric and the total normal responses on each microplane, shown in **Figs.7(a) - (c)** and **Figs.8(a) - (c)**, represents a microplane strength increase due to the volumetric response depending on confinement pressure. The difference in the triaxial compression analysis is much larger than the uniaxial compression analysis, and this difference enables the volumetric-deviatoric-shear component formulation to evaluate confinement effect.

As shown in **Fig.7(b)** and **Fig.8(b)** the total normal responses of microplane 3 are unacceptable, i.e., the microplane stress-strain curves go into the fourth quadrant of the coordinates. This means that the microplane as the basic load-carrying element at a microscopic level loses its original physical meaning as a result of resolving the normal component into the volumetric and deviatoric components. Since all microplanes in the triaxial compression analysis ultimately exhibit strain-softening responses, and unloading occurs for the volumetric component, as shown in **Figs.8(a) - (d)**, increases in macroscopic strength and ductility with confinement pressure cannot be predicted well by the volumetric-deviatoric-shear component formulation.

b) Biaxial Analysis

Fig.9 shows the stress-strain relations obtained in biaxial tension analysis with the normal-shear and volumetric-deviatoric-shear component formulations. The volumetric-deviatoric-shear component formulation predicts tensile lateral strains after a certain tensile axial strain in the uniaxial tension analysis, which implies that a uniaxial tension fracture results in lateral expansion with a negative

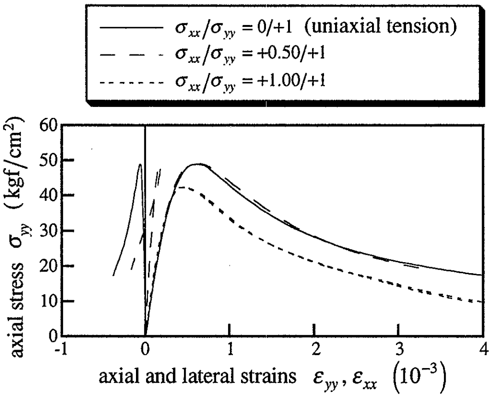

(a) Normal-shear component formulation

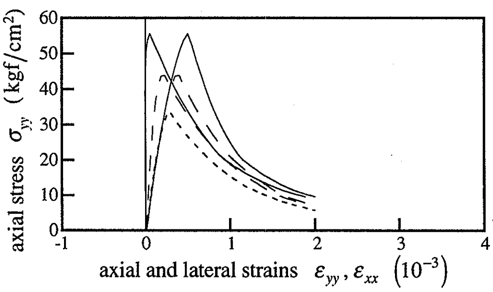

(b) Volumetric-deviatoric-shear component formulation

Fig.9 Biaxial tension analysis

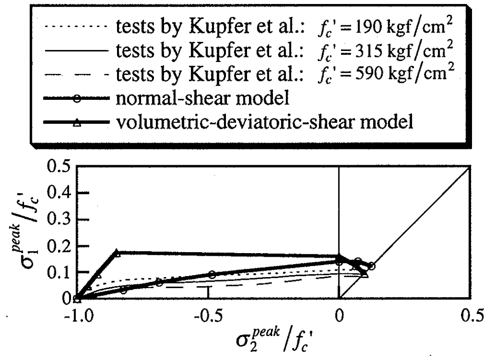

(a) Compression-tension and tension-tension stress regions

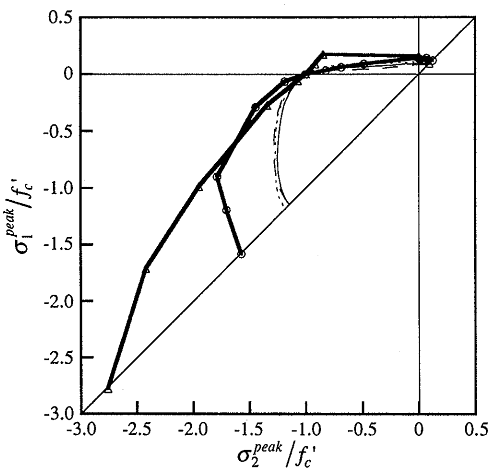

(b) Entire region of biaxial stress

Fig.10 Biaxial strength envelopes

Poisson's ratio. This is because the volumetric tensile response becomes prominent and induces volumetric expansion in uniaxial tension analysis with the volumetric-deviatoric-shear component formulation. As shown in **Fig.9(a)**, the normal-shear component formulation predicts a reasonable stress-strain relation with a positive Poisson's ratio in uniaxial tension analysis. The formulation describes the characteristic of a concrete material that peak stresses under biaxial tension are almost the same as the uniaxial tensile strength.

The biaxial strength envelopes given by the normal-shear and volumetric-deviatoric-shear component formulations are compared with experimental envelopes of Kupfer et al. [12] in **Fig.10**. The normal-shear component formulation gives a relatively good biaxial compression-tension strength envelope compared with the experiments, although the formulation predicts a slightly higher uniaxial tensile strength and somewhat overestimates biaxial compressive strengths. On the other hand, the volumetric-deviatoric-shear component formulation predicts much higher biaxial compressive strengths as well as biaxial compression-tension strengths when compared with the experiments. In analysis with the volumetric-deviatoric-shear component formulation, the peak stress of volumetric tension component is assumed to be the same as the deviatoric tension component ($\sigma_{VT}^0 = \sigma_{DT}^0$) according to the Prat model [3], in contrast with Hasegawa's study [6] where $\sigma_{VT}^0 > \sigma_{DT}^0$ was assumed to obtain a good biaxial tensile strength envelope. Therefore, biaxial tensile strengths are underestimated with the volumetric-deviatoric-shear component formulation.

3. REFORMULATION OF ENHANCED MICROPLANE CONCRETE MODEL

The volumetric-deviatoric-shear component formulation loses the conceptional clearness of the microplane because the volumetric component is used. Furthermore, the aforementioned analyses demonstrate that the model cannot predict constitutive relations under multiaxial stress conditions with accuracy. On the other hand, the normal-shear component formulation (the Hasegawa model), based on the fundamental idea of the microplane, is proven to have practically better prediction accuracy for biaxial and low confinement stress conditions; however, this model cannot describe well the strength increase and the brittle-ductile transition under high triaxial stress conditions.

In view of the finding that the normal-shear component formulation (the Hasegawa model) gives relatively better prediction accuracy than the volumetric-deviatoric-shear component formulation, an improvement to the former model is made in this second part of the present study. To develop a rational constitutive law with more general applicability, or Enhanced Microplane Concrete Model, the prediction accuracy of the Hasegawa model on confinement effect is improved by taking account of the complicated interactions between microplanes, not only for the shear components but also for the normal component.

3.1 Modification

Improvements to take account of interactions between microplanes are mentioned first.

a) Lateral Strain and Stress Effects on Normal Response of Microplane

In the Microplane Concrete Model, the normal stress increment on a microplane depends not only on the normal strain ε_N but also on the resolved lateral strain ε_L (lateral strain effect). This hypothesis means that each microplane response is determined uniquely by the microplane strains, which closely follows the basic concept of the microplane model that each microplane is independent. However, as shown in the preceding analyses, appropriate confinement effect is not obtained only with the lateral strain effect.

Due to heterogeneity resulting mainly from the existence of coarse aggregate particles, microcracks, plasticity, and damage occurring in one direction at the microscopic level in concrete affect the inelastic responses in the other directions within the concrete, and this effect forms a microscopic interaction. When the interface region between the coarse aggregate particles and the mortar matrix is compressed under the suppressed lateral strains of the region and large compressive confinement stress occurs in the lateral direction of the region, microcracks are not likely to occur. Therefore, the strength of the region increases and a plastic hardening state is reached. Since the lateral stress acting in the interface region consists of the normal stresses acting in other interface regions perpendicular to it, microscopic interactions can be modeled by taking account of lateral stresses of the interface regions, i.e., microplanes.

In the Enhanced Microplane Concrete Model interactions between microplanes relating to normal components are taken into account by assuming that the normal compression response of microplane depends on the lateral stresses S_L, which are the resolved lateral components of stress tensor σ_{ij} (lateral stress effect), in addition to the lateral strain effect (**Fig.11(d)**). The lateral strain and stress effects are also considered for hysteresis in unloading and reloading of microplane normal components.

b) Transition from Brittle to Ductile Fracture for Shear Response of Microplane

The shear peak stress τ_0 of a microplane is assumed to depend on the normal stress S_N which is the resolved normal component of the stress tensor σ_{ij} on the same microplane in the Microplane Concrete Model (dependence of shear peak stress on resolved normal stress). The shear friction law is used to describe the interactions among shear responses of microplanes through the stress tensor σ_{ij}, which is the integral of shear and normal stresses for all microplanes. As clarified in the preceding analyses, the transition from brittle to ductile fracture in concrete as confinement pressure increases cannot be described only by applying the shear friction law to the shear peak stress.

Considering the shear frictional phenomenon at a microscopic level in concrete, a microcrack tends to close and does not develop further when the normal compression stress on the plane of the microcrack

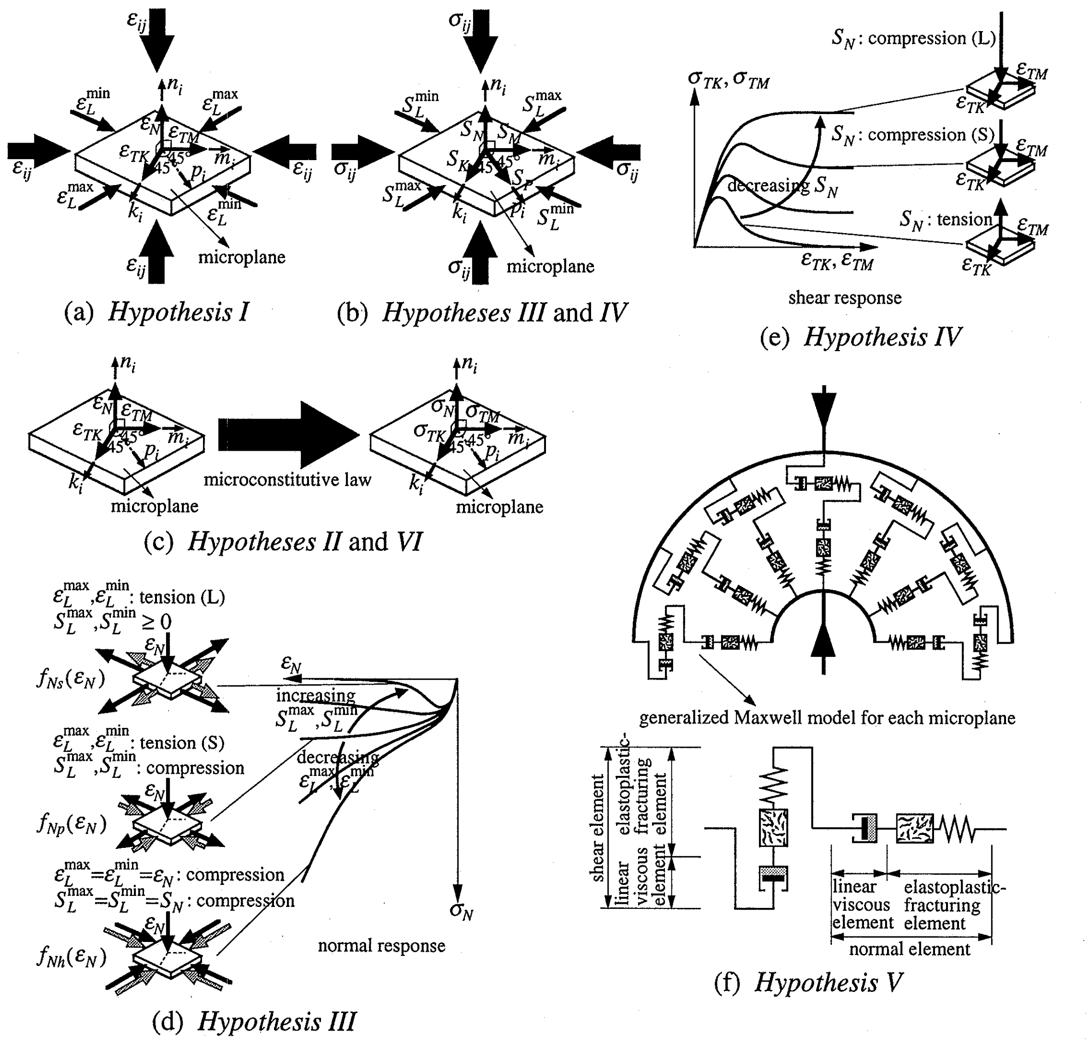

Fig.11 Hypotheses of Enhanced Microplane Concrete Model

increases, i.e., when the confinement pressure increases. Then the microscopic shear response becomes more plastic, and the post-peak shear response changes from brittle softening to ductile plastic behavior.

In the Enhanced Microplane Concrete Model, the interactions between microplanes relating to shear components are taken into account in terms of the shear friction law, in that the shear peak stress and ductility of microplanes increase with the resolved normal compression stress on the same microplane (transition from brittle to ductile fracture for microplane shear response)(**Fig.11(e)**). A similar transition model is also considered for hysteresis in unloading and reloading of microplane shear components.

3.2 Hypotheses

The aforementioned interactions between microplanes are taken into account as *Hypotheses III* and *IV* in the Enhanced Microplane Concrete Model. The following are the hypotheses made in the present model:
Hypothesis I : Normal strain ε_N, shear strains ε_{TK}, ε_{TM}, and lateral strain ε_L of a microplane are the resolved components of the macroscopic strain tensor ε_{ij} (tensorial kinematic constraint).
Hypothesis II : Normal stress σ_N and shear stresses σ_{TK}, σ_{TM} on a microplane depend on normal strain ε_N and shear strains ε_{TK}, ε_{TM}. The relations between those strains and stresses are described by

microconstitutive laws. The directions of the shear stresses on each microplane are the same as those of the shear strains.
Hypothesis III : The inelastic normal stress increment on a microplane depends on the resolved lateral strain ε_L of the macroscopic strain tensor ε_{ij} (lateral strain effect) and resolved lateral stress S_L of the macroscopic stress tensor σ_{ij} onto the same microplane (additional static constraint: lateral stress effect).
Hypothesis IV : The inelastic shear stress increment on a microplane depends on the resolved normal component S_N of the macroscopic stress tensor σ_{ij} onto the same microplane (additional static constraint: transition from brittle to ductile fracture for microplane shear response).
Hypothesis V : The microconstitutive laws for the normal and shear components are based on a generalized Maxwell rheologic model in which a linear viscous element is coupled in series with an elastoplastic-fracturing element.
Hypothesis VI : The microconstitutive laws for the normal and shear components on each microplane are mutually independent.
Fig.11 illustrates these hypotheses.

3.3 Basic Formulation

a) Microplane Strains

According to *Hypothesis I*, the normal strain component on a microplane with unit normal vector $\mathbf{n}$ is

$$\varepsilon_N = n_j \varepsilon_j^n = n_j n_k \varepsilon_{jk} \tag{5}$$

in which n_i = components of unit normal vector $\mathbf{n}$ of the microplane.

For *Hypotheses I* and *II*, two in-plane unit coordinate vectors $\mathbf{k}$ and $\mathbf{m}$, normal to each other, are introduced on each microplane as shown in **Fig.11(a)**, and two shear strain components ε_{TK}, ε_{TM} in those directions are considered. Since the directions of the vectors $\mathbf{k}$ and $\mathbf{m}$ must be fixed at the beginning of calculations, some kind of rule to determine these directions is necessary. The rule must not have a significant bias for any direction, i.e., the frequency of various directions within the microplanes taken by vectors $\mathbf{m}$ and $\mathbf{n}$ must be about the same. This is approximately achieved by the following simple rule: vector $\mathbf{m}$ of microplane 1 is determined to be normal to the z-axis, vector $\mathbf{m}$ of microplane 2 normal to the x-axis, vector $\mathbf{m}$ of microplane 3 normal to y-axis, vector $\mathbf{m}$ of microplane 4 normal again to the z-axis, and so on. The x-, y-, and z-axes are a set of three mutually orthogonal axes in the Cartesian coordinate system x_i. Then for vector $\mathbf{m}$ normal to z-axis

$$m_1 = \frac{n_2}{\sqrt{n_1^2 + n_2^2}}; \qquad m_2 = \frac{-n_1}{\sqrt{n_1^2 + n_2^2}}; \qquad m_3 = 0 \tag{6a}$$

but $m_1 = 1$; $m_2 = 0$; $m_3 = 0$ if $n_1 = n_2 = 0$.
For vector $\mathbf{m}$ normal to x-axis

$$m_2 = \frac{n_3}{\sqrt{n_2^2 + n_3^2}}; \qquad m_3 = \frac{-n_2}{\sqrt{n_2^2 + n_3^2}}; \qquad m_1 = 0 \tag{6b}$$

but $m_1 = 0$; $m_2 = 1$; $m_3 = 0$ if $n_2 = n_3 = 0$.
For vector $\mathbf{m}$ normal to y-axis

$$m_1 = \frac{-n_3}{\sqrt{n_1^2 + n_3^2}}; \qquad m_3 = \frac{n_1}{\sqrt{n_1^2 + n_3^2}}; \qquad m_2 = 0 \tag{6c}$$

but $m_1 = 0$; $m_2 = 0$; $m_3 = 1$ if $n_1 = n_3 = 0$.

After determining vector $\mathbf{m}$, vector $\mathbf{k}$ is calculated for each microplane as $\mathbf{k} = \mathbf{m} \times \mathbf{n}$. The shear strain components in the $\mathbf{k}$ and $\mathbf{m}$ directions on a microplane with direction cosines n_i are

$$\varepsilon_{TK} = k_j \varepsilon_j^n = k_j n_i \varepsilon_{ij} = \frac{1}{2}\left(k_i n_j + k_j n_i\right)\varepsilon_{ij} \tag{7a}$$

$$\varepsilon_{TM} = m_j \varepsilon_j^n = m_j n_i \varepsilon_{ij} = \frac{1}{2}\left(m_i n_j + m_j n_i\right)\varepsilon_{ij} \tag{7b}$$

where the symmetry of ε_{ij} is exploited to symmetrize these expressions. k_i and m_i are components of in-plane unit coordinate vectors $\mathbf{k}$ and $\mathbf{m}$.

To implement *Hypothesis III*, we need derive equations for the maximum and minimum principal values $\varepsilon_L^{\max}$, $\varepsilon_L^{\min}$ of lateral strain of each microplane. To this end we introduce another in-plane unit vector $\mathbf{p}$ whose angle with the unit vectors $\mathbf{k}$ and $\mathbf{m}$ is 45°, as shown in **Fig.11(a)**; $\mathbf{p}=(\mathbf{k}+\mathbf{m})/\sqrt{2}$. The lateral normal strains in the directions of $\mathbf{k}$, $\mathbf{m}$, and $\mathbf{p}$ are

$$\varepsilon_K = k_i k_j \varepsilon_{ij} \tag{8a}$$

$$\varepsilon_M = m_i m_j \varepsilon_{ij} \tag{8b}$$

$$\varepsilon_P = p_i p_j \varepsilon_{ij} \tag{8c}$$

in which p_i = components of the in-plane unit vector $\mathbf{p}$ of the microplane.
Considering Mohr's circle for the in-plane strains of the microplane, we can obtain the maximum and minimum principal values $\varepsilon_L^{\max}$, $\varepsilon_L^{\min}$ of the lateral strain on each microplane

$$\varepsilon_L^{\max} = \frac{\varepsilon_K+\varepsilon_M}{2} + \sqrt{\left(\frac{\varepsilon_K-\varepsilon_M}{2}\right)^2 + \left(\frac{\varepsilon_K+\varepsilon_M}{2}-\varepsilon_P\right)^2} \tag{9a}$$

$$\varepsilon_L^{\min} = \frac{\varepsilon_K+\varepsilon_M}{2} - \sqrt{\left(\frac{\varepsilon_K-\varepsilon_M}{2}\right)^2 + \left(\frac{\varepsilon_K+\varepsilon_M}{2}-\varepsilon_P\right)^2} \tag{9b}$$

b) Incremental Form of Macroscopic Stress-Strain Relation

As with (1) for the previous model [6], the incremental forms of microconstitutive relations are written separately for the normal component and the shear components in the *K* and *M* directions:

normal component: $d\sigma_N = C_N d\varepsilon_N - d\sigma_N'' = f_{N1}(\varepsilon_N, \varepsilon_L, S_L) = f_{N2}(\varepsilon_{kl}, \sigma_{kl}, n_r)$ (10a)

K-shear component: $d\sigma_{TK} = C_{TK} d\varepsilon_{TK} - d\sigma_{TK}'' = f_{T1}(\varepsilon_{TK}, S_N) = f_{T2}(\varepsilon_{kl}, \sigma_{kl}, n_r)$ (10b)

M-shear component: $d\sigma_{TM} = C_{TM} d\varepsilon_{TM} - d\sigma_{TM}'' = f_{T1}(\varepsilon_{TM}, S_N) = f_{T2}(\varepsilon_{kl}, \sigma_{kl}, n_r)$ (10c)

in which $f_{N1}(\varepsilon_N, \varepsilon_L, S_L)$ and $f_{N2}(\varepsilon_{kl}, \sigma_{kl}, n_r)$ are microplane normal stress increments $d\sigma_N$ expressed in terms of ε_N, ε_L, and S_L, and in terms of ε_{kl}, σ_{kl}, and n_r; $f_{T1}(\varepsilon_{Ts}, S_N)$ and $f_{T2}(\varepsilon_{kl}, \sigma_{kl}, n_r)$ are microplane shear stress increments $d\sigma_{Ts}$ expressed in terms of ε_{Ts} and S_N, and in terms of ε_{kl}, σ_{kl}, and n_r $(Ts = TK, TM)$.

Using the principle of virtual work (i.e., the equality of virtual works of the stress tensor within a unit sphere and microplane stresses on the surface of the sphere), we can write

$$\frac{4\pi}{3} d\sigma_{ij} \delta\varepsilon_{ij} = 2\int_S (d\sigma_N \delta\varepsilon_N + d\sigma_{TK}\delta\varepsilon_{TK} + d\sigma_{TM}\delta\varepsilon_{TM}) f(\mathbf{n}) dS \tag{11}$$

in which $\int_S dS = \int_0^{2\pi}\int_0^{\pi/2} \sin\phi\, d\phi\, d\theta$; θ and ϕ = the spherical angular coordinates; and $\delta\varepsilon_{ij}$, $\delta\varepsilon_N$, $\delta\varepsilon_{TK}$, and $\delta\varepsilon_{TM}$ = small variations of the strain tensor and of the microplane strains. The constant $4\pi/3$ means that the work of the stress tensor is taken over the volume of the unit sphere. The factor of 2 on the right-hand side arises because the work of microplanes needs to be integrated only over the surface of the unit hemisphere S. The function $f(\mathbf{n})$ is a weight function for the normal directions $\mathbf{n}$, which in general can be used to introduce anisotropy of the material in its initial state. We will use $f(\mathbf{n})=1$, which means isotropy. Expressing $\delta\varepsilon_N$, $\delta\varepsilon_{TK}$, and $\delta\varepsilon_{TM}$ from (5) and (7) and substituting them into (11), we obtain

$$\frac{4\pi}{3} d\sigma_{ij}\delta\varepsilon_{ij} = 2\int_S \left[n_i n_j d\sigma_N + \frac{d\sigma_{TK}}{2}(k_i n_j + k_j n_i) + \frac{d\sigma_{TM}}{2}(m_i n_j + m_j n_i)\right] f(\mathbf{n}) dS \delta\varepsilon_{ij} \tag{12}$$

This variational equation must hold for any variations $\delta\varepsilon_{ij}$, therefore, we can delete $\delta\varepsilon_{ij}$. Then, substituting (10), we obtain

$$d\sigma_{ij} = \frac{3}{2\pi}\int_S \left[n_i n_j (C_N d\varepsilon_N - d\sigma_N'') + \frac{1}{2}(k_i n_j + k_j n_i)(C_{TK} d\varepsilon_{TK} - d\sigma_{TK}'') + \frac{1}{2}(m_i n_j + m_j n_i)(C_{TM} d\varepsilon_{TM} - d\sigma_{TM}'')\right] f(\mathbf{n}) dS \tag{13}$$

(5) and (7) may now be here substituted for ε_N, ε_{TK}, and ε_{TM}. This finally yields the incremental form of the macroscopic stress-strain relation, which is the same as (2) in the previous model

$$d\sigma_{ij} = C_{ijrs} d\varepsilon_{rs} - d\sigma_{ij}'' \tag{14a}$$

$$C_{ijrs} = \frac{3}{2\pi}\int_S \Big[n_i n_j n_r n_s C_N + \frac{1}{4}\left(k_i n_j + k_j n_i\right)\left(k_r n_s + k_s n_r\right) C_{TK} + \frac{1}{4}\left(m_i n_j + m_j n_i\right)\left(m_r n_s + m_s n_r\right) C_{TM} \Big] f(\mathbf{n}) dS \tag{14b}$$

$$d\sigma_{ij}'' = \frac{3}{2\pi}\int_S \Big[n_i n_j d\sigma_N'' + \frac{1}{2}\left(k_i n_j + k_j n_i\right) d\sigma_{TK}'' + \frac{1}{2}\left(m_i n_j + m_j n_i\right) d\sigma_{TM}'' \Big] f(\mathbf{n}) dS \tag{14c}$$

in which C_{ijrs} = incremental elastic stiffness tensor; and $d\sigma_{ij}''$ = inelastic stress increment.

Relation (14) can be expressed in another form (15).

$$\begin{aligned} d\sigma_{ij} &= \frac{3}{2\pi}\int_S \Big[n_i n_j d\sigma_N + \frac{d\sigma_{TK}}{2}\left(k_i n_j + k_j n_i\right) + \frac{d\sigma_{TM}}{2}\left(m_i n_j + m_j n_i\right) \Big] f(\mathbf{n}) dS \\ &= \frac{3}{2\pi}\int_S \Big[n_i n_j f_{N2}(\varepsilon_{kl}, \sigma_{kl}, n_r) + \frac{1}{2}\left(k_i n_j + k_j n_i\right) f_{T2}(\varepsilon_{kl}, \sigma_{kl}, n_r) \\ &\quad + \frac{1}{2}\left(m_i n_j + m_j n_i\right) f_{T2}(\varepsilon_{kl}, \sigma_{kl}, n_r) \Big] f(\mathbf{n}) dS \end{aligned} \tag{15}$$

As can be seen from the fact that the incremental stress tensor $d\sigma_{ij}$ depends not only on strain tensor ε_{kl} but also on stress tensor σ_{kl}, the interactions between microplanes are modeled in the Enhanced Microplane Concrete Model through the additional static constraint that a microplane response depends on the resolved components of the stress tensor obtained by spherical integration of the stresses of all microplanes. This interaction effect means that the present model deviates from the basic concept that individual microplane responses are mutually independent, which leads to the kinematic constraint. This is necessary to take account of a situation within concrete where microcracks, damage, and plasticity in each direction have mutual effects.

For the initial isotropic elastic response, we can substitute the initial moduli C_N^0 and C_T^0 for C_N and C_{TK}, C_{TM} in (14b) and set $f(\mathbf{n}) = 1$. Since these moduli are independent of the microplane direction, we could integrate (14b) explicitly if the unit vectors **k** and **m** were also known explicitly. However, they are not explicit, being calculated numerically as described before. For initial elasticity we can substitute the initial moduli C_N^0 and C_T^0 for C_N and C_{TK}, C_{TM} in (10) and set $d\sigma_N'' = d\sigma_{TK}'' = d\sigma_{TM}'' = 0$. Then we have $d\sigma_{TK} = C_T^0 d\varepsilon_{TK}$ and $d\sigma_{TM} = C_T^0 d\varepsilon_{TM}$ for shears. From that, $|d\sigma_T| = C_T^0 |d\varepsilon_T|$, where $|d\sigma_T| = \sqrt{d\sigma_{TK}^2 + d\sigma_{TM}^2}$ and $|d\varepsilon_T| = \sqrt{d\varepsilon_{TK}^2 + d\varepsilon_{TM}^2}$. This is the same relation as that used in the previous microplane model by Bazant and Kim [1] involving normal and shear components (in which the shear vectors were characterized by three components in the Cartesian coordinates x_i; $i = 1, 2, 3$). Therefore the expressions derived in that study apply

$$C_N^0 = \frac{E^0}{\left(1 - 2\nu^0\right)} \tag{16a}$$

$$C_T^0 = \frac{\left(1 - 4\nu^0\right) E^0}{\left(1 - 2\nu^0\right)\left(1 + \nu^0\right)} \tag{16b}$$

in which E^0 and ν^0 are Young's modulus and Poisson's ratio.

c) Rheologic Model for Rate Effect in Microconstitutive Law

The present model is a rate-dependent constitutive law as a consequence of adopting a series coupling of a linear viscous element and an elastoplastic-fracturing element for the microconstitutive law on each microplane according to *Hypothesis V* (**Fig.11(f)**). For the sake of brevity of notation, let ε and σ now represent any of the microplane strains ε_N, ε_{TK}, and ε_{TM}, and microplane stresses σ_N, σ_{TK}, and σ_{TM}, respectively. The generalized Maxwell rheologic model is described by the differential equation

$$\frac{d\sigma}{dt} = C^t \frac{d\varepsilon}{dt} - \frac{\sigma}{\rho} \tag{17}$$

where C^t is the current tangent stiffness of the elastoplastic-fracturing element, which takes the value of either C^v or C^{ur} depending on the loading-unloading-reloading criteria described later; $C^t = C^v$ for virgin loading and $C^t = C^{ur}$ for unloading and reloading; t = time; and ρ = relaxation time of the viscous element. If (17) is solved by using a central difference approximation, numerical difficulties or instabilities may be encountered in the case of strain softening, and even if the solution is numerically stable, a large error is usually accumulated and the stress is not reduced exactly to zero at very large strains.

To overcome these difficulties in the Microplane Concrete Model [6], a numerical method of solving this equation was conceived based on the exponential algorithm [14] initially developed for aging creep of concrete. This method is used again here. Considering the initial condition for the numerical time duration (from the previous time step t_r to the present time step t_{r+1}) in the general solution of (17), and taking the values $C^{ur}_{r+1/2}$, $C^{t}_{r+1/2}$, and $\sigma_{r+1/2}$ for the middle of the duration, denoted with subscript $r+1/2$, the incremental solution of (17) is obtained in the form of the microconstitutive relations (10)

$$\Delta\sigma = C\Delta\varepsilon - \Delta\sigma'' \tag{18a}$$

$$C = \frac{1}{\Delta z}\left(1 - e^{-\Delta z}\right)C^{ur}_{r+1/2} \tag{18b}$$

$$\Delta\sigma'' = \left(1 - e^{-\Delta z}\right)\sigma_r \tag{18c}$$

$$\Delta z = \Delta t / \beta_{r+1/2} \tag{19}$$

$$\frac{1}{\beta_{r+1/2}} = \frac{1}{\rho} + \left(C^{ur}_{r+1/2} - C^{t}_{r+1/2}\right)\sigma_{r+1/2}\frac{\Delta\varepsilon}{\Delta t} \tag{20}$$

in which σ_r = microplane stress at the previous time step t_r.

3.4 Microconstitutive Law for Normal Components

Aside from the hydrostatic compression response, the lateral-deviatoric strain ε_{LD}, which is the difference between normal ε_N and lateral ε_L strains of a microplane, increases with loading until it finally reaches infinity due to the macroscopic Poisson effect. In the Microplane Concrete Model the lateral strain effect on the normal compression response of a microplane is modeled so that the normal compression response becomes softening when the lateral-deviatoric strain ε_{LD} approaches infinity. However, since the normal compression response of microplane is softening due to a monotonic increase in lateral-deviatoric strain even in the case of triaxial compression analysis under high confinement pressure, perfect plastic behavior and transition from brittle to ductile fracture are not obtained on the macroscopic level. In the present model this problem is circumvented by *Hypothesis III*. The purpose of taking account the lateral strain and stress effects on normal compression response of a microplane according to *Hypothesis III* is to achieve the following (**Fig.11(d)**):

1) The normal compression response would not be the same as the hydrostatic response except when the lateral strains ε_L are the same as the normal strain ε_N, which is the case of hydrostatic loading.
2) The normal compression response would have a plastic plateau when the difference between the normal strain ε_N and the lateral strain ε_L is large and the resolved lateral stress S_L of the microplane is a large, compressive value, i.e., it would exhibit ductile plasticity.
3) The normal compression response would be more brittle when the difference between the normal strain ε_N and the lateral strain ε_L is large and the resolved lateral stress S_L of the microplane is a small, compressive value or a tensile value, i.e., it would exhibit more strain softening.

a) Hardening-Softening Function for Microplane

To formulate the lateral stress effect, we resolve the stress tensor σ_{ij} into the lateral normal stresses S_K, S_M, and S_P in the directions of the in-plane unit coordinate vectors $\mathbf{k}$, $\mathbf{m}$, and $\mathbf{p}$ (**Fig.11(b)**)

$$S_K = k_i k_j \sigma_{ij} \tag{21a}$$

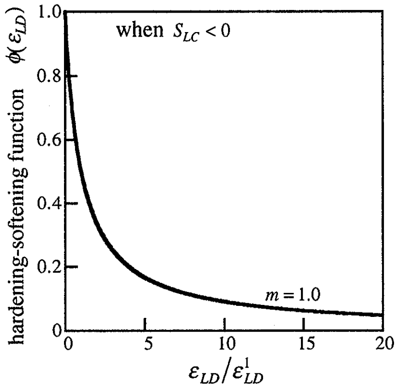

Fig.12 Hardening-softening function for normal compression

$$S_M = m_i m_j \sigma_{ij} \tag{21b}$$

$$S_P = p_i p_j \sigma_{ij} \tag{21c}$$

Considering Mohr's circle for the lateral normal stresses of the microplane, we can obtain the maximum and minimum principal values $S_L^{\max}$, $S_L^{\min}$ of the lateral stress of each microplane

$$S_L^{\max} = \frac{S_K + S_M}{2} + \sqrt{\left(\frac{S_K - S_M}{2}\right)^2 + \left(\frac{S_K + S_M}{2} - S_P\right)^2} \tag{22a}$$

$$S_L^{\min} = \frac{S_K + S_M}{2} - \sqrt{\left(\frac{S_K - S_M}{2}\right)^2 + \left(\frac{S_K + S_M}{2} - S_P\right)^2} \tag{22b}$$

We define a lateral confinement stress S_{LC} that combines $S_L^{\max}$ and $S_L^{\min}$ into one stress invariant for the microplane

$$\begin{aligned} S_{LC} &= S_L^{\max} + S_L^{\min} && : \text{when } S_L^{\max} < 0 \text{ and } S_L^{\min} < 0 \\ &= 0 && : \text{when } S_L^{\max} \geq 0 \\ &= 0 && : \text{when } S_N \geq 0 \text{ on any other microplane} \\ &= S_{LC}^p && : \text{when } S_{LC} \leq S_{LC}^p \end{aligned} \tag{23}$$

in which $S_{LC}^p \leq S_{LC} \leq 0$; and S_{LC}^p = S_{LC} value corresponding to the case of plastic response.

The lateral-deviatoric strain ε_{LD}, which is the difference between the normal ε_N and lateral ε_L strains of a microplane, is defined using the maximum and minimum principal values $\varepsilon_L^{\max}$, $\varepsilon_L^{\min}$ of the lateral strain on the microplane

$$\varepsilon_{LD} = \left|\varepsilon_N - \varepsilon_L^{\max}\right| + \left|\varepsilon_N - \varepsilon_L^{\min}\right| \tag{24}$$

In the present model, the following hardening-softening function $\phi(\varepsilon_{LD})$ based on the lateral-deviatoric strain ε_{LD} and the lateral confinement stress S_{LC} is introduced (**Fig.12**):

$$\begin{aligned} \phi(\varepsilon_{LD}) &= \frac{1}{1 + \left(\varepsilon_{LD}/\varepsilon_{LD}^1\right)^m} && : \text{when } S_{LC} < 0 \\ &= \phi^p && : \text{when } \varepsilon_{LD} = \varepsilon_{LD}^p \\ &= 0 && : \text{when } S_{LC} \geq 0 \end{aligned} \tag{25}$$

in which ε_{LD}^1 = ε_{LD} value when $\phi(\varepsilon_{LD}) = 0.5$; ε_{LD}^p = ε_{LD} value corresponding to the case of normal plastic response; m = a constant that specifies the shape of the curve $\phi(\varepsilon_{LD})$; and ϕ^p = $\phi(\varepsilon_{LD})$ value corresponding to the case of normal plastic response.

b) Lateral Strain and Stress Effects

Weight functions are defined in terms of $\phi(\varepsilon_{LD})$ and S_{LC}, and utilized to obtain a gradual transition from hydrostatic response to plastic response and softening response for the virgin loading curve of the normal component of the microplane (**Fig.11(d)**).

When $1 \geq \phi(\varepsilon_{LD}) \geq \phi^p$ and any S_{LC}:

$$\sigma_N(\varepsilon_N, \varepsilon_{LD}, S_{LC}) = \left(\frac{\phi(\varepsilon_{LD}) - \phi^p}{1-\phi^p}\right) f_{Nh}(\varepsilon_N) + \left(\frac{1-\phi(\varepsilon_{LD})}{1-\phi^p}\right) f_{Np}(\varepsilon_N) \tag{26a}$$

when $\phi^p > \phi(\varepsilon_{LD}) \geq 0$ and $S_{LC} \leq S_{LC}^p$:

$$\sigma_N(\varepsilon_N, \varepsilon_{LD}, S_{LC}) = f_{Np}(\varepsilon_N) \tag{26b}$$

when $\phi^p > \phi(\varepsilon_{LD}) \geq 0$ and $S_{LC}^p < S_{LC} < 0$:

$$\sigma_N(\varepsilon_N, \varepsilon_{LD}, S_{LC}) = \left(\frac{S_{LC}}{S_{LC}^p}\right) f_{Np}(\varepsilon_N) + \left(\frac{S_{LC}^p - S_{LC}}{S_{LC}^p}\right) f_{Ns}(\varepsilon_N) \tag{26c}$$

when $\phi^p > \phi(\varepsilon_{LD}) \geq 0$ and $0 \leq S_{LC}$:

$$\sigma_N(\varepsilon_N, \varepsilon_{LD}, S_{LC}) = f_{Ns}(\varepsilon_N) \tag{26d}$$

in which $f_{Nh}(\varepsilon_N)$ = hydrostatic loading curve (when $\phi(\varepsilon_{LD}) = 1$); $f_{Np}(\varepsilon_N)$ = plastic loading curve (when $\phi(\varepsilon_{LD}) = \phi^p$); and $f_{Ns}(\varepsilon_N)$ = compression softening loading curve (when $\phi^p > \phi(\varepsilon_{LD}) \geq 0$ and $0 \leq S_{LC}$).

To obtain the loading tangent stiffness for normal compression response, we need to differentiate (26). Thus,

when $1 \geq \phi(\varepsilon_{LD}) \geq \phi^p$ and any S_{LC}:

$$\frac{\partial \sigma_N(\varepsilon_N, \varepsilon_{LD}, S_{LC})}{\partial \varepsilon_N} = \left(\frac{\phi(\varepsilon_{LD}) - \phi^p}{1-\phi^p}\right) \frac{df_{Nh}(\varepsilon_N)}{d\varepsilon_N} + \left(\frac{1-\phi(\varepsilon_{LD})}{1-\phi^p}\right) \frac{df_{Np}(\varepsilon_N)}{d\varepsilon_N} \tag{27a}$$

when $\phi^p > \phi(\varepsilon_{LD}) \geq 0$ and $S_{LC} \leq S_{LC}^p$:

$$\frac{\partial \sigma_N(\varepsilon_N, \varepsilon_{LD}, S_{LC})}{\partial \varepsilon_N} = \frac{df_{Np}(\varepsilon_N)}{d\varepsilon_N} \tag{27b}$$

when $\phi^p > \phi(\varepsilon_{LD}) \geq 0$ and $S_{LC}^p < S_{LC} < 0$:

$$\frac{\partial \sigma_N(\varepsilon_N, \varepsilon_{LD}, S_{LC})}{\partial \varepsilon_N} = \left(\frac{S_{LC}}{S_{LC}^p}\right) \frac{df_{Np}(\varepsilon_N)}{d\varepsilon_N} + \left(\frac{S_{LC}^p - S_{LC}}{S_{LC}^p}\right) \frac{df_{Ns}(\varepsilon_N)}{d\varepsilon_N} \tag{27c}$$

when $\phi^p > \phi(\varepsilon_{LD}) \geq 0$ and $0 \leq S_{LC}$:

$$\frac{\partial \sigma_N(\varepsilon_N, \varepsilon_{LD}, S_{LC})}{\partial \varepsilon_N} = \frac{df_{Ns}(\varepsilon_N)}{d\varepsilon_N} \tag{27d}$$

Similarly, the transition for the linear unload-reload stiffnesses $C_N^{ur0}(\sigma_N^u, \varepsilon_N^u, \varepsilon_{LD}^{ur}, S_{LC}^{ur})$ may be written as follows.

When $1 \geq \phi(\varepsilon_{LD}) \geq \phi^p$ and any S_{LC}:

$$C_N^{ur0}(\sigma_N^u, \varepsilon_N^u, \varepsilon_{LD}^{ur}, S_{LC}^{ur}) = \left(\frac{\phi(\varepsilon_{LD}^{ur}) - \phi^p}{1-\phi^p}\right) C_{Nh}^{ur0}(\sigma_N^u, \varepsilon_N^u) + \left(\frac{1-\phi(\varepsilon_{LD}^{ur})}{1-\phi^p}\right) C_{Np}^{ur0}(\sigma_N^u, \varepsilon_N^u) \tag{28a}$$

when $\phi^p > \phi(\varepsilon_{LD}) \geq 0$ and $S_{LC} \leq S_{LC}^p$:

$$C_N^{ur0}(\sigma_N^u, \varepsilon_N^u, \varepsilon_{LD}^{ur}, S_{LC}^{ur}) = C_{Np}^{ur0}(\sigma_N^u, \varepsilon_N^u) \tag{28b}$$

when $\phi^p > \phi(\varepsilon_{LD}) \geq 0$ and $S_{LC}^p < S_{LC} < 0$:

$$C_N^{ur0}(\sigma_N^u, \varepsilon_N^u, \varepsilon_{LD}^{ur}, S_{LC}^{ur}) = \left(\frac{S_{LC}^{ur}}{S_{LC}^p}\right) C_{Np}^{ur0}(\sigma_N^u, \varepsilon_N^u) + \left(\frac{S_{LC}^p - S_{LC}^{ur}}{S_{LC}^p}\right) C_{Ns}^{ur0}(\sigma_N^u, \varepsilon_N^u) \tag{28c}$$

when $\phi^p > \phi(\varepsilon_{LD}) \geq 0$ and $0 \leq S_{LC}$:

$$C_N^{ur0}(\sigma_N^u, \varepsilon_N^u, \varepsilon_{LD}^{ur}, S_{LC}^{ur}) = C_{Ns}^{ur0}(\sigma_N^u, \varepsilon_N^u) \tag{28d}$$

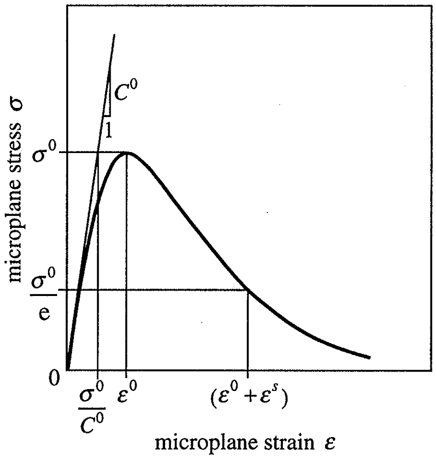

Fig.13 Softening loading curve for microplane

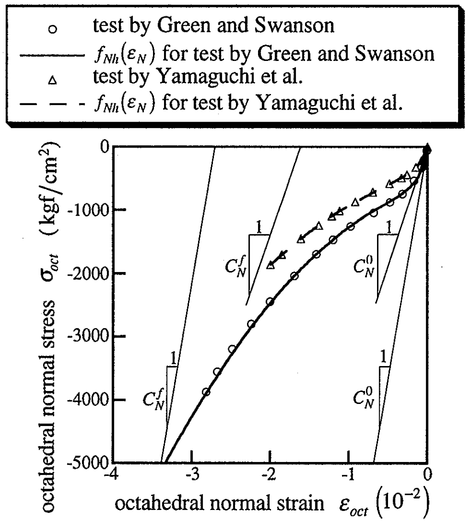

Fig.14 Hydrostatic loading curve for microplane and comparison with experiments

in which $C_{Nh}^{ur0}(\sigma_N^u, \varepsilon_N^u)$ = the linear unload-reload stiffness for the hydrostatic loading curve (when $\phi(\varepsilon_{LD}^{ur}) = 1$); $C_{Np}^{ur0}(\sigma_N^u, \varepsilon_N^u)$ = the linear unload-reload stiffness for the plastic loading curve (when $\phi(\varepsilon_{LD}^{ur}) = \phi^p$); $C_{Ns}^{ur0}(\sigma_N^u, \varepsilon_N^u)$ = the linear unload-reload stiffness for the compression softening loading curve (when $\phi^p > \phi(\varepsilon_{LD}^{ur}) \geq 0$ and $0 \leq S_{LC}^{ur}$); σ_N^u and ε_N^u = the normal stress and strain at the start of unloading; ε_{LD}^{ur} = the lateral-deviatoric strain for unloading and reloading (ε_{LD} value corresponding to the start of unloading); and S_{LC}^{ur} = the lateral confinement stress for unloading and reloading (S_{LC} value corresponding to the start of unloading).

This model incorporates interactions between microplanes by taking into account the lateral strain and stress effects in the normal compression response of a microplane using (26), (27), and (28).

c) Loading Curves for Normal Component

In the previous microplane models of Prat [3], Gambarova [2], and Oh [15], virgin loading curves for strain softening on each microplane are formulated using a single exponential function. With this kind of equation, however, one cannot adjust the peak stress, peak strain, and the post-peak ductility individually. To do so in this study we use two separate virgin loading curves for pre-peak and post-peak regions, as in the Microplane Concrete Model.

The virgin loading curves for the pre-peak and post-peak tensile regions of the normal component are (**Fig.13**)

for $0 \leq \varepsilon_N \leq \varepsilon_{NT}^0$ (pre-peak):

$$\sigma_N = \sigma_{NT}^0 \left[1 - \left(1 - \frac{\varepsilon_N}{\varepsilon_{NT}^0} \right)^{C_N^0 \varepsilon_{NT}^0 / \sigma_{NT}^0} \right] \tag{29a}$$

for $\varepsilon_{NT}^0 < \varepsilon_N$ (post-peak):

$$\sigma_N = \sigma_{NT}^0 \exp\left[-\left(\frac{\varepsilon_N - \varepsilon_{NT}^0}{\varepsilon_{NT}^s} \right)^{p_{NT}} \right] \tag{29b}$$

in which $\varepsilon_{NT}^0 = \dfrac{\sigma_{NT}^0}{\zeta_{NT} C_N^0}$; and $\varepsilon_{NT}^s = \gamma_{NT} \varepsilon_{NT}^0 = \dfrac{\gamma_{NT} \sigma_{NT}^0}{\zeta_{NT} C_N^0}$. In (29), σ_{NT}^0 is the peak stress of the curve,

ζ_{NT} is a parameter that controls the peak strain ε_{NT}^0, and γ_{NT} is a parameter that controls ε_{NT}^s. At the strain $\varepsilon_N = \varepsilon_{NT}^0 + \varepsilon_{NT}^s$, the stress σ_N decreases to σ_{NT}^0/e in the softening region. p_{NT} is a parameter that changes the shape of the softening loading curve. Thus we can control the shape of the stress-strain curve with these four parameters quite easily, which is important for the proper adjustment of the macroscopic response with the microplane model.

For the compression range of the normal component, we must specify the equations for the hydrostatic, plastic, and compression softening loading curves, as mentioned before. For the hydrostatic loading curve of the normal component, we use (30) (**Fig.14**).

$$f_{Nh}(\varepsilon_N) = \sigma_N = \left[\frac{C_N^0}{\left(\dfrac{\varepsilon_N C_N^0}{\sigma_a}\right)^{p_H} + 1} + \frac{C_N^f}{\left(\dfrac{\varepsilon_N C_N^f}{2\sigma_b}\right)^{-q_H} + 1} \right] \varepsilon_N \tag{30}$$

in which $\sigma_a = C_N^0 \varepsilon_a$; $\sigma_b = C_N^f \varepsilon_b / 2$; C_N^f = the asymptotic final modulus for normal compression; σ_a and σ_b = the normal stresses corresponding to ε_a and ε_b; ε_a and ε_b = normal strain values that characterize the shape of the curve; and p_H and q_H = exponents which also change the shape $(p_H \le 1$, $q_H > -1)$.

For the plastic loading curve of the normal component, (31) is adopted.
For $0 \ge \varepsilon_N \ge \varepsilon_{Np}^0$ (pre-peak):

$$f_{Np}(\varepsilon_N) = \sigma_N = \sigma_{Np}^0 \left[1 - \left(1 - \frac{\varepsilon_N}{\varepsilon_{Np}^0} \right)^{C_N^0 \varepsilon_{Np}^0 / \sigma_{Np}^0} \right] \tag{31a}$$

for $\varepsilon_{Np}^0 > \varepsilon_N$ (post-peak):

$$f_{Np}(\varepsilon_N) = \sigma_N = \sigma_{Np}^0 \tag{31b}$$

in which $\varepsilon_{Np}^0 = \dfrac{\sigma_{Np}^0}{\zeta_{Np} C_N^0}$. In (31) σ_{Np}^0 and ε_{Np}^0 are the peak stress and the peak strain, and ζ_{Np} is a parameter that controls ε_{Np}^0.

The same types of equation as for tension are assumed as for compression softening of the normal component (**Fig.13**)
for $0 \ge \varepsilon_N \ge \varepsilon_{NC}^0$ (pre-peak):

$$f_{Ns}(\varepsilon_N) = \sigma_N = \sigma_{NC}^0 \left[1 - \left(1 - \frac{\varepsilon_N}{\varepsilon_{NC}^0} \right)^{C_N^0 \varepsilon_{NC}^0 / \sigma_{NC}^0} \right] \tag{32a}$$

for $\varepsilon_{NC}^0 > \varepsilon_N$ (post-peak):

$$f_{Ns}(\varepsilon_N) = \sigma_N = \sigma_{NC}^0 \exp\left[-\left(\frac{\varepsilon_N - \varepsilon_{NC}^0}{\varepsilon_{NC}^s} \right)^{p_{NC}} \right] \tag{32b}$$

in which $\varepsilon_{NC}^0 = \dfrac{\sigma_{NC}^0}{\zeta_{NC} C_N^0}$; and $\varepsilon_{NC}^s = \gamma_{NC} \varepsilon_{NC}^0 = \dfrac{\gamma_{NC} \sigma_{NC}^0}{\zeta_{NC} C_N^0}$.

Fig.15 gives the calculated results of normal compression response with this model, showing the lateral strain and stress effects. As the figure shows, there is a transition from brittle to ductile fracture, in which the residual strength after the peak stress increases with confinement between the compression softening and plastic loading curves. In **Fig.14** calculated hydrostatic compression behavior using (30) is compared with the experimental data of Green and Swanson [16] as well as of Yamaguchi et al.

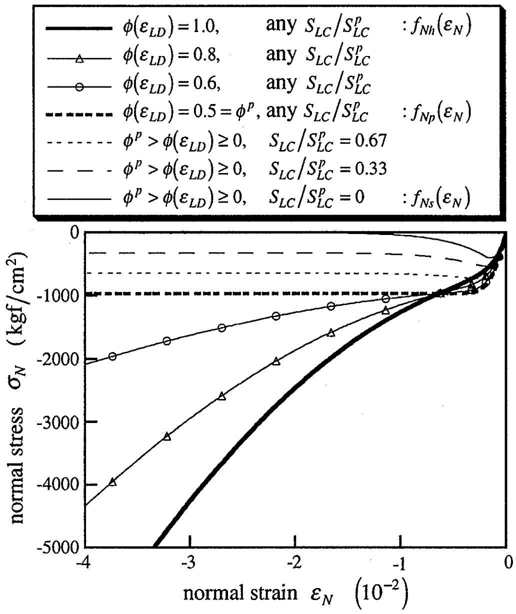

Fig.15 Lateral strain and stress effects on normal compression response of a microplane

[17]. The material parameters identified are $C_N^f = C_N^0$, $\sigma_a = -965\ \mathrm{kgf/cm^2}$, $\sigma_b = -63060\ \mathrm{kgf/cm^2}$, and $p_H = q_H = 1.0$ for Green and Swanson, and $C_N^f = C_N^0$, $\sigma_a = -700\ \mathrm{kgf/cm^2}$, $\sigma_b = -19000\ \mathrm{kgf/cm^2}$, and $p_H = q_H = 1.0$ for Yamaguchi et al. From the comparison, we can conclude that (30) can predict the hydrostatic compression behavior of concrete with accuracy.

d) Linear Unload-Reload Stiffness

The hysteresis rule for unloading and reloading of a microplane is based on the linear unload-reload stiffness C^{ur0} as described later.

As the linear unload-reload stiffnesses $C_{Nh}^{ur0}(\sigma_N^u,\varepsilon_N^u)$, $C_{Np}^{ur0}(\sigma_N^u,\varepsilon_N^u)$ of the normal component for the hydrostatic loading curve and for the plastic loading curve, the initial modulus C_N^0 for the normal component is used without taking into consideration stiffness degradation due to damage.

$$C_{Nh}^{ur0}(\sigma_N^u,\varepsilon_N^u) = C_N^0 \tag{33}$$

$$C_{Np}^{ur0}(\sigma_N^u,\varepsilon_N^u) = C_N^0 \tag{34}$$

In the pre-peak region of the tensile or compressive softening response for the normal component, C_N^0 is used as the linear unload-reload stiffnesses $C_{NT}^{ur0}(\sigma_N^u,\varepsilon_N^u)$, $C_{Ns}^{ur0}(\sigma_N^u,\varepsilon_N^u)$. On the other hand, after the peak stress of the tensile or compressive softening response, the following damage evolution is assumed for linear unload-reload stiffnesses $C_{NT}^{ur0}(\sigma_N^u,\varepsilon_N^u)$, $C_{Ns}^{ur0}(\sigma_N^u,\varepsilon_N^u)$:

For $0 \le \varepsilon_{NT}^u \le \varepsilon_{NT}^0$ (pre-peak tension):

$$C_{NT}^{ur0}(\sigma_N^u,\varepsilon_N^u) = C_N^0 \tag{35a}$$

for $\varepsilon_{NT}^u > \varepsilon_{NT}^0$ (post-peak tension):

$$C_{NT}^{ur0}(\sigma_N^u,\varepsilon_N^u) = \alpha_{NT}C_N^0 + (1-\alpha_{NT})\frac{\sigma_{NT}^u}{\varepsilon_{NT}^u - \xi_{NT}} \tag{35b}$$

for $0 \ge \varepsilon_{NC}^u \ge \varepsilon_{NC}^0$ (pre-peak compression):

$$C_{Ns}^{ur0}(\sigma_N^u,\varepsilon_N^u) = C_N^0 \tag{35c}$$

for $\varepsilon_{NC}^{u} < \varepsilon_{NC}^{0}$ (post-peak compression):

$$C_{Ns}^{ur0}\left(\sigma_N^u, \varepsilon_N^u\right) = \alpha_{NC} C_N^0 + \left(1 - \alpha_{NC}\right) \frac{\sigma_{NC}^u}{\varepsilon_{NC}^u - \xi_{NC}} \tag{35d}$$

in which $\xi_{NT} = \varepsilon_{NT}^0 - \dfrac{\sigma_{NT}^0}{C_N^0}$; $\xi_{NC} = \varepsilon_{NC}^0 - \dfrac{\sigma_{NC}^0}{C_N^0}$; σ_{NT}^u and σ_{NC}^u = the normal stresses at the start of unloading for tension and compression softenings; ε_{NT}^u and ε_{NC}^u = the normal strains at the start of unloading for tension and compression softenings; α_{NT} and α_{NC} = weight constants which describe the proportions of progressive damage in tension and compression softenings; and ξ_{NT} and ξ_{NC} = plastic residual strains after complete unloading with C_N^0 from the peak stress to zero stress. Thus, using the linear unload-reload stiffnesses $C_{NT}^{ur0}\left(\sigma_N^u, \varepsilon_N^u\right)$, $C_{Ns}^{ur0}\left(\sigma_N^u, \varepsilon_N^u\right)$, which are formulated with α_{NT} and α_{NC} representing damage of microplane and with ξ_{NT} and ξ_{NC} taking account of microplane plasticity, we can control the elastoplastic-fracturing behavior for the case of softening in the normal microplane component.

3.5 Microconstitutive Law for Shear Components

Since the difference between K-shear and M-shear is only its direction on the microplane, the microconstitutive laws for those shears must be identical. Therefore, we do not differentiate K-shear from M-shear, but consider a unique microconstitutive law for shear with subscript T which refers to K-shear (TK) and M-shear (TM).

a) Transition from Brittle to Ductile Fracture with Confinement

In the present model, shear loading curves are defined individually for softening (subscript TT) under resolved normal tension stress, softening (subscript TC) under resolved normal compression stress, and plasticity (subscript Tp) under resolved normal compression stress. A shear friction law is applied to evaluate shear peak stress for pre-peak and post-peak curves under resolved normal tension stress and for pre-peak curves under resolved normal compression stress. On the other hand, post-peak shear response under resolved normal compression stress is calculated by weighting the softening and plasticity loading curves with resolved normal stress. This results in a transition model from brittle to ductile fracture for shear response on the microplane (**Fig.11(e)**).

The resolved normal component S_N of the stress tensor σ_{ij} on a microplane whose direction cosines are n_i is

$$S_N = n_j \sigma_j^n = n_j n_k \sigma_{jk} \tag{36}$$

The loading curve $\sigma_T\left(\varepsilon_T, S_N\right)$ under resolved normal stress S_N is calculated by weighting each loading curve $f_{Tp}\left(\varepsilon_T\right)$, $f_{TC}\left(\varepsilon_T\right)$, and $f_{TT}\left(\varepsilon_T\right)$ with resolved normal stress S_N as follows.

When $S_N \le S_N^p$:

$$\sigma_T\left(\varepsilon_T, S_N\right) = f_{Tp}\left(\varepsilon_T\right) \tag{37a}$$

when $S_N^p < S_N < 0$ and in pre-peak:

$$\sigma_T\left(\varepsilon_T, S_N\right) = f_{TC}\left(\varepsilon_T\right) = f_{Tp}\left(\varepsilon_T\right) \tag{37b}$$

when $S_N^p < S_N < 0$ and in post-peak:

$$\sigma_T\left(\varepsilon_T, S_N\right) = \left(\frac{S_N}{S_N^p}\right) f_{Tp}\left(\varepsilon_T\right) + \left(\frac{S_N^p - S_N}{S_N^p}\right) f_{TC}\left(\varepsilon_T\right) \tag{37c}$$

when $0 \le S_N$:

$$\sigma_T\left(\varepsilon_T, S_N\right) = f_{TT}\left(\varepsilon_T\right) \tag{37d}$$

in which $f_{Tp}\left(\varepsilon_T\right)$ = plastic loading curve (when $S_N \le S_N^p$); $f_{TC}\left(\varepsilon_T\right)$ and $f_{TT}\left(\varepsilon_T\right)$ = softening loading curves under resolved normal compression and tension stresses; and S_N^p = S_N value when the shear response corresponds to the plastic loading curve.

The loading tangent stiffness for shear response is obtained by differentiating (37).

When $S_N \le S_N^p$:

$$\frac{\partial \sigma_T(\varepsilon_T, S_N)}{\partial \varepsilon_T} = \frac{df_{Tp}(\varepsilon_T)}{d\varepsilon_T} \tag{38a}$$

when $S_N^p < S_N < 0$ and in pre-peak:

$$\frac{\partial \sigma_T(\varepsilon_T, S_N)}{\partial \varepsilon_T} = \frac{df_{TC}(\varepsilon_T)}{d\varepsilon_T} = \frac{df_{Tp}(\varepsilon_T)}{d\varepsilon_T} \tag{38b}$$

when $S_N^p < S_N < 0$ and in post-peak:

$$\frac{\partial \sigma_T(\varepsilon_T, S_N)}{\partial \varepsilon_T} = \left(\frac{S_N}{S_N^p}\right)\frac{df_{Tp}(\varepsilon_T)}{d\varepsilon_T} + \left(\frac{S_N^p - S_N}{S_N^p}\right)\frac{df_{TC}(\varepsilon_T)}{d\varepsilon_T} \tag{38c}$$

when $0 \le S_N$:

$$\frac{\partial \sigma_T(\varepsilon_T, S_N)}{\partial \varepsilon_T} = \frac{df_{TT}(\varepsilon_T)}{d\varepsilon_T} \tag{38d}$$

Similarly, the linear unload-reload stiffness $C_T^{ur0}(\sigma_T^u, \varepsilon_T^u, S_N^{ur})$ is calculated

when $S_N \le S_N^p$:

$$C_T^{ur0}(\sigma_T^u, \varepsilon_T^u, S_N^{ur}) = C_{Tp}^{ur0}(\sigma_T^u, \varepsilon_T^u) \tag{39a}$$

when $S_N^p < S_N < 0$ and in pre-peak:

$$C_T^{ur0}(\sigma_T^u, \varepsilon_T^u, S_N^{ur}) = C_{TC}^{ur0}(\sigma_T^u, \varepsilon_T^u) = C_{Tp}^{ur0}(\sigma_T^u, \varepsilon_T^u) \tag{39b}$$

when $S_N^p < S_N < 0$ and in post-peak:

$$C_T^{ur0}(\sigma_T^u, \varepsilon_T^u, S_N^{ur}) = \left(\frac{S_N^{ur}}{S_N^p}\right) C_{Tp}^{ur0}(\sigma_T^u, \varepsilon_T^u) + \left(\frac{S_N^p - S_N^{ur}}{S_N^p}\right) C_{TC}^{ur0}(\sigma_T^u, \varepsilon_T^u) \tag{39c}$$

when $0 \le S_N$:

$$C_T^{ur0}(\sigma_T^u, \varepsilon_T^u, S_N^{ur}) = C_{TT}^{ur0}(\sigma_T^u, \varepsilon_T^u) \tag{39d}$$

in which $C_{Tp}^{ur0}(\sigma_T^u, \varepsilon_T^u)$ = the linear unload-reload stiffness for the plastic loading curve (when $S_N^{ur} \le S_N^p$); $C_{TC}^{ur0}(\sigma_T^u, \varepsilon_T^u)$ = the linear unload-reload stiffness for the softening loading curve under resolved normal compression stress; $C_{TT}^{ur0}(\sigma_T^u, \varepsilon_T^u)$ = the linear unload-reload stiffness for the softening loading curve under resolved normal tension stress; σ_T^u and ε_T^u = the shear stress and strain at the start of unloading; and S_N^{ur} = the resolved normal stress for unloading and reloading (S_N value corresponding to the start of unloading).

b) Loading Curves for Shear Components

The softening loading curve $f_{TT}(\varepsilon_T)$ under resolved normal tension stress is

for $0 \le |\varepsilon_T| \le |\varepsilon_{TT}^0|$ (pre-peak):

$$f_{TT}(\varepsilon_T) = \sigma_T = \tau^0\left[1 - \left(1 - \frac{\varepsilon_T}{\varepsilon_{TT}^0}\right)^{C_T^0 \varepsilon_{TT}^0/\tau^0}\right] \tag{40a}$$

for $|\varepsilon_{TT}^0| < |\varepsilon_T|$ (post-peak):

$$f_{TT}(\varepsilon_T) = \sigma_T = \tau^0 \exp\left[-\left(\frac{\varepsilon_T - \varepsilon_{TT}^0}{\varepsilon_{TT}^s}\right)^{p_{TT}}\right] \tag{40b}$$

in which $\varepsilon_{TT}^0 = \dfrac{\tau^0}{\zeta_{TT} C_T^0}$; $\varepsilon_{TT}^s = \gamma_{TT}\varepsilon_{TT}^0 = \dfrac{\gamma_{TT}\tau^0}{\zeta_{TT} C_T^0}$; and τ^0 = shear peak stress, which depends on the resolved normal stress S_N.

The softening loading curve $f_{TT}(\varepsilon_T)$ under resolved normal compression stress is
for $0 \le |\varepsilon_T| \le |\varepsilon_{TC}^0|$ (pre-peak):

$$f_{TC}(\varepsilon_T) = \sigma_T = \tau^0\left[1-\left(1-\frac{\varepsilon_T}{\varepsilon_{TC}^0}\right)^{C_T^0\varepsilon_{TC}^0/\tau^0}\right] \tag{41a}$$

for $|\varepsilon_{TC}^0| < |\varepsilon_T|$ (post-peak):

$$f_{TC}(\varepsilon_T) = \sigma_T = \tau^0 \exp\left[-\left(\frac{\varepsilon_T - \varepsilon_{TC}^0}{\varepsilon_{TC}^s}\right)^{p_{TC}}\right] \tag{41b}$$

in which $\varepsilon_{TC}^0 = \dfrac{\tau^0}{\zeta_{TC}C_T^0}$; and $\varepsilon_{TC}^s = \gamma_{TC}\varepsilon_{TC}^0 = \dfrac{\gamma_{TC}\tau^0}{\zeta_{TC}C_T^0}$.

The plastic loading curve $f_{Tp}(\varepsilon_T)$ under resolved normal compression stress is
for $0 \le |\varepsilon_T| \le |\varepsilon_{TC}^0|$ (pre-peak):

$$f_{Tp}(\varepsilon_T) = \sigma_T = \tau^0\left[1-\left(1-\frac{\varepsilon_T}{\varepsilon_{TC}^0}\right)^{C_T^0\varepsilon_{TC}^0/\tau^0}\right] \tag{42a}$$

for $|\varepsilon_{TC}^0| < |\varepsilon_T|$ (post-peak):

$$f_{Tp}(\varepsilon_T) = \sigma_T = \tau^0 \tag{42b}$$

Unlike the normal component, (40), (41), and (42) are applied to both tension and compression. The only difference between tension and compression is the sign of the peak stress τ^0, i.e., $\tau^0 > 0$ in tension $(\varepsilon_T > 0)$ and $\tau^0 < 0$ in compression $(\varepsilon_T < 0)$. The concept of shear frictional coefficient μ_{TT}, μ_{TC} is utilized to model the dependence of shear peak stress τ^0 on resolved normal stress S_N.
For tension of shear $(\varepsilon_T > 0)$:

when $S_N < 0$: $\tau^0 = +\sigma_{TC}^0 - \mu_{TC}S_N$ (43a)

when $S_N \ge 0$: $\tau^0 = +\sigma_{TT}^0 - \mu_{TT}S_N \ge +r_{\min}^0\sigma_{TT}^0$ (43b)

for compression of shear $(\varepsilon_T < 0)$:

when $S_N < 0$: $\tau^0 = -\sigma_{TC}^0 + \mu_{TC}S_N$ (43c)

when $S_N \ge 0$: $\tau^0 = -\sigma_{TT}^0 + \mu_{TT}S_N \le -r_{\min}^0\sigma_{TT}^0$ (43d)

in which $\sigma_{TT}^0(>0)$ and $\sigma_{TC}^0(>0)$ = shear peak stresses at $S_N = 0$ under resolved normal tension and compression stresses; $\mu_{TT}(>0)$ and $\mu_{TC}(>0)$ = shear frictional coefficients under resolved normal tension and compression stresses; and $r_{\min}^0$ = a constant specifying a lower limit on shear peak stress under resolved normal tension stress $(0 < r_{\min}^0 \le 1)$.

Fig.16 shows calculated shear responses under resolved normal tension and compression stresses with this model, where there is a transition from brittle to ductile fracture.

c) Linear Unload-Reload Stiffness

As the linear unload-reload stiffness $C_{Tp}^{ur0}(\sigma_T^u, \varepsilon_T^u)$ of the shear component for the plastic loading curve, the initial modulus C_T^0 for the shear component is used without considering stiffness degradation due to damage.

$$C_{Tp}^{ur0}(\sigma_T^u, \varepsilon_T^u) = C_T^0 \tag{44}$$

In the pre-peak region of the softening response for the shear component, C_T^0 is used as the linear unload-reload stiffnesses $C_{TT}^{ur0}(\sigma_T^u, \varepsilon_T^u)$, $C_{TC}^{ur0}(\sigma_T^u, \varepsilon_T^u)$ under resolved normal tension and compression

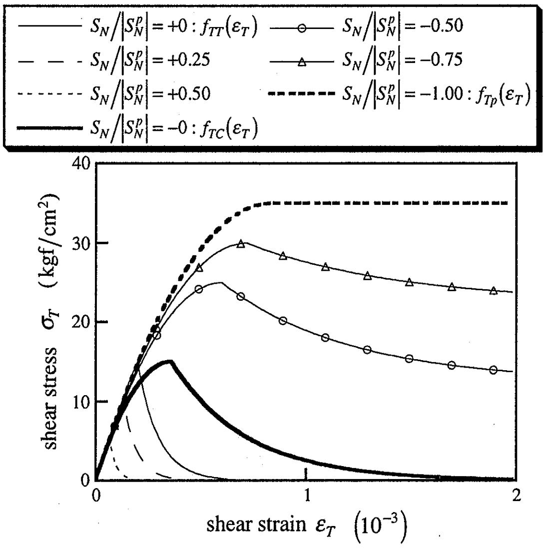

Fig.16 Transition from brittle to ductile fracture for shear response of a microplane

stresses. On the other hand, after the peak stress of the softening response, the following damage evolution is assumed for linear unload-reload stiffnesses $C_{TT}^{ur0}\left(\sigma_T^u, \varepsilon_T^u\right)$, $C_{TC}^{ur0}\left(\sigma_T^u, \varepsilon_T^u\right)$ under resolved normal tension and compression stresses:

For $0 \le \left|\varepsilon_T^u\right| \le \left|\varepsilon_{TT}^0\right|$ and $S_N^{ur} \ge 0$ (pre-peak):

$$C_{TT}^{ur0}\left(\sigma_T^u, \varepsilon_T^u\right) = C_T^0 \tag{45a}$$

for $\left|\varepsilon_{TT}^0\right| < \left|\varepsilon_T^u\right|$ and $S_N^{ur} \ge 0$ (post-peak):

$$C_{TT}^{ur0}\left(\sigma_T^u, \varepsilon_T^u\right) = \alpha_{TT} C_T^0 + \left(1 - \alpha_{TT}\right) \frac{\sigma_T^u}{\varepsilon_T^u - \xi_{TT}} \tag{45b}$$

for $0 \le \left|\varepsilon_T^u\right| \le \left|\varepsilon_{TC}^0\right|$ and $S_N^{ur} < 0$ (pre-peak):

$$C_{TC}^{ur0}\left(\sigma_T^u, \varepsilon_T^u\right) = C_T^0 \tag{45c}$$

for $\left|\varepsilon_{TC}^0\right| < \left|\varepsilon_T^u\right|$ and $S_N^{ur} < 0$ (post-peak):

$$C_{TC}^{ur0}\left(\sigma_T^u, \varepsilon_T^u\right) = \alpha_{TC} C_T^0 + \left(1 - \alpha_{TC}\right) \frac{\sigma_T^u}{\varepsilon_T^u - \xi_{TC}} \tag{45d}$$

in which $\xi_{TT} = \varepsilon_{TT}^0 - \dfrac{\tau^0}{C_T^0}$; and $\xi_{TC} = \varepsilon_{TC}^0 - \dfrac{\tau^0}{C_T^0}$.

3.6 Loading, Unloading and Reloading in Microconstitutive Relations

With the most of phenomenologic constitutive models, loading, unloading, or reloading has to be judged in general stress and strain tensor conditions. In the case of theories of plasticity and damage mechanics, loading functions, plastic potential functions, or damage potential functions are formulated using invariants calculated with stress and strain tensors. Loading, unloading, or reloading is judged using these functions. However, it is not easy to establish appropriate loading criteria for cases when the principal directions rotate or neutral loading occurs, for which the invariants are not adequate. On the other hand, the Enhanced Microplane Concrete Model does not require loading criteria for stress and strain tensors, but needs loading criteria in the microconstitutive relations between microplane stress and microplane strain. These are scalar variables since cross effects among microplane components are not taken into account. Therefore, the criteria for loading, unloading, and reloading are very simple in the present model, which gives an advantage over phenomenologic constitutive models.

Let each microplane strain ε_N, ε_{TK}, ε_{TM} and microplane stress σ_N, σ_{TK}, σ_{TM} be defined as ε and σ for the sake of simplicity. The following loading-unloading-reloading criteria are used for all the components:

Loading:

when $\sigma_r > 0$ (tension), $\quad \Delta\varepsilon_{r+1} > 0, \quad \varepsilon_{r+1} \geq \varepsilon_{\max}$ (46a)

when $\sigma_r < 0$ (compression), $\quad \Delta\varepsilon_{r+1} < 0, \quad \varepsilon_{r+1} \leq \varepsilon_{\min}$ (46b)

Unloading:

when $\sigma_r > 0$ (tension), $\quad \Delta\varepsilon_{r+1} < 0, \quad \varepsilon_{r+1} < \varepsilon_{\max}$ (46c)

when $\sigma_r < 0$ (compression), $\quad \Delta\varepsilon_{r+1} > 0, \quad \varepsilon_{r+1} > \varepsilon_{\min}$ (46d)

Reloading:

when $\sigma_r > 0$ (tension), $\quad \Delta\varepsilon_{r+1} > 0, \quad \varepsilon_{r+1} < \varepsilon_{\max}$ (46e)

when $\sigma_r < 0$ (compression), $\quad \Delta\varepsilon_{r+1} < 0, \quad \varepsilon_{r+1} > \varepsilon_{\min}$ (46f)

in which σ_r = microplane stress of each component at the end of the previous load step; ε_{r+1} = microplane strain of each component at the present load step; $\Delta\varepsilon_{r+1}$ = microplane strain increment of each component $\left(\Delta\varepsilon_{r+1} = \varepsilon_{r+1} - \varepsilon_r\right)$; ε_r = microplane strain of each component at the end of the previous load step; and $\varepsilon_{\max}$ and $\varepsilon_{\min}$ = the maximum and minimum values of microplane strain in the history. In (46) $\varepsilon_{\max}$ and $\varepsilon_{\min}$ are considered as scalar potentials for loading.

3.7 Hysteresis Rule for Microconstitutive Relations

The linear unload-reload stiffnesses $C_N^{ur0}\left(\sigma_N^u, \varepsilon_N^u, \varepsilon_{LD}^{ur}, S_{LC}^{ur}\right)$ in (28) and $C_{NT}^{ur0}\left(\sigma_N^u, \varepsilon_N^u\right)$ in (35a), (35b) for the normal component as well as the linear unload-reload stiffness $C_T^{ur0}\left(\sigma_T^u, \varepsilon_T^u, S_N^{ur}\right)$ in (39) for the shear component can be used with the loading-unloading-reloading criteria in (46), to describe the cyclic behavior of each component. However, numerical simulations with $C_N^{ur0}\left(\sigma_N^u, \varepsilon_N^u, \varepsilon_{LD}^{ur}, S_{LC}^{ur}\right)$, $C_{NT}^{ur0}\left(\sigma_N^u, \varepsilon_N^u\right)$, and $C_T^{ur0}\left(\sigma_T^u, \varepsilon_T^u, S_N^{ur}\right)$ reveal that the hysteresis loops are too narrow in the macroscopic responses. Wider hysteresis loops on the microplane are necessary to obtain proper hysteresis on the macroscopic level. The reason for this is that hysteresis loops govern the energy dissipation, and the basic hypothesis of the microplane model is energy equivalence between the macroscopic and microscopic levels.

To obtain macroscopic hysteresis in the Microplane Concrete Model [6], a hysteresis rule with microplane back-stress and objective-stress was developed. The microplane back-stress and objective-stress were conceived on the basis of a concept analogous to the kinematic hardening rule in plasticity theory to describe inelastic behavior in unloading and reloading. Although in the kinematic hardening rule the back-stress is defined as the center of the loading surface, the microplane back-stress and objective-stress in this hysteresis rule are the microplane stresses at the start and end of inelastic behavior in unloading and reloading. A single value of the microplane back-stress is used for both unloading and reloading; it is updated to the microplane stress at the end of the previous load step whenever the sign of the microplane strain increment is reversed during calculations. When a monotonic unloading or reloading occurs on a microplane, the hysteresis rule works well. However, when unloading and reloading occur in turn on a microplane, the microplane back-stress is always set equal to the microplane stress at the end of the previous load step, and the tangent stiffness becomes its maximum value. Then the hysteresis loop becomes narrow or does not occur.

In this study the microplane back-stress is redefined separately for unloading and reloading to prevent the hysteresis loops from becoming narrow as described above. Furthermore, lateral strain and stress effects are taken into account in the microplane hysteresis response during unloading and reloading in normal compression, and a resolved normal stress dependence of the microplane hysteresis response for the shear component is formulated. In the following, the microplane strains ε_N, ε_{TK}, ε_{TM} and microplane stresses σ_N, σ_{TK}, σ_{TM} are defined as ε and σ for the sake of simplicity.

a) Back-Stress, Objective-Stress and Unloading-Reloading Function

The microplane back-stresses $\sigma^U_{b,r+1}$, $\sigma^R_{b,r+1}$ for unloading and reloading are defined as follows.

When $\Delta\varepsilon_r \cdot \Delta\varepsilon_{r+1} < 0$, $|\varepsilon^R_{b,r}| \le |\varepsilon_{r+1}|$: $\quad \sigma^U_{b,r+1} = \sigma_r$ (47a)

when $\Delta\varepsilon_r \cdot \Delta\varepsilon_{r+1} < 0$, $|\varepsilon^R_{b,r}| > |\varepsilon_{r+1}|$: $\quad \sigma^U_{b,r+1} = \sigma^u$ (47b)

when $\Delta\varepsilon_r \cdot \Delta\varepsilon_{r+1} \ge 0$, $|\varepsilon^R_{b,r}| \le |\varepsilon_{r+1}|$: $\quad \sigma^U_{b,r+1} = \sigma^U_{b,r}$ (47c)

when $\Delta\varepsilon_r \cdot \Delta\varepsilon_{r+1} \ge 0$, $|\varepsilon^R_{b,r}| > |\varepsilon_{r+1}|$: $\quad \sigma^U_{b,r+1} = \sigma^u$ (47d)

when $\Delta\varepsilon_r \cdot \Delta\varepsilon_{r+1} < 0$, $|\varepsilon^U_{b,r}| \ge |\varepsilon_{r+1}|$: $\quad \sigma^R_{b,r+1} = \sigma_r$ (47e)

when $\Delta\varepsilon_r \cdot \Delta\varepsilon_{r+1} < 0$, $|\varepsilon^U_{b,r}| < |\varepsilon_{r+1}|$: $\quad \sigma^R_{b,r+1} = 0$ (47f)

when $\Delta\varepsilon_r \cdot \Delta\varepsilon_{r+1} \ge 0$, $|\varepsilon^U_{b,r}| \ge |\varepsilon_{r+1}|$: $\quad \sigma^R_{b,r+1} = \sigma^R_{b,r}$ (47g)

when $\Delta\varepsilon_r \cdot \Delta\varepsilon_{r+1} \ge 0$, $|\varepsilon^U_{b,r}| < |\varepsilon_{r+1}|$: $\quad \sigma^R_{b,r+1} = 0$ (47h)

in which $\sigma^U_{b,r+1}$, $\sigma^U_{b,r}$ = microplane back-stresses for unloading at the present and previous load steps; $\sigma^R_{b,r+1}$, $\sigma^R_{b,r}$ = microplane back-stresses for reloading at the present and previous load steps; $\varepsilon^U_{b,r}$ = microplane strain corresponding to the microplane back-stress for unloading at the previous load step; $\varepsilon^R_{b,r}$ = microplane strain corresponding to the microplane back-stress for reloading at the previous load step; σ_r = microplane stress at the previous load step; σ^u = microplane stress at the start of unloading; ε_{r+1} = microplane strain at the present load step; and $\Delta\varepsilon_{r+1}$ and $\Delta\varepsilon_r$ = microplane strain increments at the present and previous load steps.

The microplane objective-stress σ_{ob} is defined as

when unloading: $\quad \sigma_{ob} = 0$ (48a)

when reloading: $\quad \sigma_{ob} = \sigma^u$ (48b)

The microplane back-stresses $\sigma^U_{b,r+1}$, $\sigma^R_{b,r+1}$ and the microplane objective-stress σ_{ob} are set according to (47) and (48) when the unloading or reloading criteria are satisfied. The unloading-reloading function $F^{ur}(\sigma)$, which is nondimensional, is defined for the microplane stress σ during unloading or reloading.

When unloading: $$F^{ur}(\sigma) = \left| \frac{\sigma^U_{b,r+1} - \sigma}{\sigma_{ob} - \sigma^U_{b,r+1}} \right| \tag{49a}$$

when reloading: $$F^{ur}(\sigma) = \left| \frac{\sigma^R_{b,r+1} - \sigma}{\sigma_{ob} - \sigma^R_{b,r+1}} \right| \tag{49b}$$

in which $0 \le F^{ur}(\sigma) \le 1$.

b) Hysteresis Rule for Normal Component

To take into account lateral strain and stress effects on the microplane hysteresis response during unloading and reloading in normal compression, nondimensional coefficients $U_{\max}$, $U_{\min}$, $R_{\max}$, and $R_{\min}$ are defined separately for unloading from, and for reloading to, the hydrostatic, plastic, and compression softening loading curves. Weighting these coefficients, the coefficients corresponding to the hardening-softening function ϕ^{ur} and the lateral confinement stress S^{ur}_{LC} for unloading and reloading are calculated using a method similar to the virgin loading curve described in **3.4 b)**.

When $1 \ge \phi^{ur} \ge \phi^p$ and any S^{ur}_{LC}:

$$U_{\max}\left(\phi^{ur}, S^{ur}_{LC}\right) = \left(\frac{\phi^{ur} - \phi^p}{1 - \phi^p}\right) U^{Nh}_{\max} + \left(\frac{1 - \phi^{ur}}{1 - \phi^p}\right) U^{Np}_{\max} \tag{50a}$$

$$U_{\min}\left(\phi^{ur}, S^{ur}_{LC}\right) = \left(\frac{\phi^{ur} - \phi^p}{1 - \phi^p}\right) U^{Nh}_{\min} + \left(\frac{1 - \phi^{ur}}{1 - \phi^p}\right) U^{Np}_{\min} \tag{50b}$$

$$R_{\max}\left(\phi^{ur}, S^{ur}_{LC}\right) = \left(\frac{\phi^{ur} - \phi^p}{1 - \phi^p}\right) R^{Nh}_{\max} + \left(\frac{1 - \phi^{ur}}{1 - \phi^p}\right) R^{Np}_{\max} \tag{50c}$$

$$R_{\min}\left(\phi^{ur}, S_{LC}^{ur}\right) = \left(\frac{\phi^{ur} - \phi^{p}}{1-\phi^{p}}\right) R_{\min}^{Nh} + \left(\frac{1-\phi^{ur}}{1-\phi^{p}}\right) R_{\min}^{Np} \tag{50d}$$

when $\phi^p > \phi^{ur} \geq 0$ and $S_{LC}^{ur} \leq S_{LC}^{p}$:

$$U_{\max}\left(\phi^{ur}, S_{LC}^{ur}\right) = U_{\max}^{Np} \tag{50e}$$

$$U_{\min}\left(\phi^{ur}, S_{LC}^{ur}\right) = U_{\min}^{Np} \tag{50f}$$

$$R_{\max}\left(\phi^{ur}, S_{LC}^{ur}\right) = R_{\max}^{Np} \tag{50g}$$

$$R_{\min}\left(\phi^{ur}, S_{LC}^{ur}\right) = R_{\min}^{Np} \tag{50h}$$

when $\phi^p > \phi^{ur} \geq 0$ and $S_{LC}^{p} < S_{LC}^{ur} < 0$:

$$U_{\max}\left(\phi^{ur}, S_{LC}^{ur}\right) = \left(\frac{S_{LC}^{ur}}{S_{LC}^{p}}\right) U_{\max}^{Np} + \left(\frac{S_{LC}^{p} - S_{LC}^{ur}}{S_{LC}^{p}}\right) U_{\max}^{Ns} \tag{50i}$$

$$U_{\min}\left(\phi^{ur}, S_{LC}^{ur}\right) = \left(\frac{S_{LC}^{ur}}{S_{LC}^{p}}\right) U_{\min}^{Np} + \left(\frac{S_{LC}^{p} - S_{LC}^{ur}}{S_{LC}^{p}}\right) U_{\min}^{Ns} \tag{50j}$$

$$R_{\max}\left(\phi^{ur}, S_{LC}^{ur}\right) = \left(\frac{S_{LC}^{ur}}{S_{LC}^{p}}\right) R_{\max}^{Np} + \left(\frac{S_{LC}^{p} - S_{LC}^{ur}}{S_{LC}^{p}}\right) R_{\max}^{Ns} \tag{50k}$$

$$R_{\min}\left(\phi^{ur}, S_{LC}^{ur}\right) = \left(\frac{S_{LC}^{ur}}{S_{LC}^{p}}\right) R_{\min}^{Np} + \left(\frac{S_{LC}^{p} - S_{LC}^{ur}}{S_{LC}^{p}}\right) R_{\min}^{Ns} \tag{50l}$$

when $\phi^p > \phi^{ur} \geq 0$ and $0 \leq S_{LC}^{ur}$:

$$U_{\max}\left(\phi^{ur}, S_{LC}^{ur}\right) = U_{\max}^{Ns} \tag{50m}$$

$$U_{\min}\left(\phi^{ur}, S_{LC}^{ur}\right) = U_{\min}^{Ns} \tag{50n}$$

$$R_{\max}\left(\phi^{ur}, S_{LC}^{ur}\right) = R_{\max}^{Ns} \tag{50o}$$

$$R_{\min}\left(\phi^{ur}, S_{LC}^{ur}\right) = R_{\min}^{Ns} \tag{50p}$$

in which $U_{\max}^{Nh}$, $U_{\max}^{Np}$, $U_{\max}^{Ns}$ = nondimensional coefficients determining the maximum unloading tangent stiffness $C_{\max}^{u} = U_{\max}\left(\phi^{ur}, S_{LC}^{ur}\right) \cdot C_N^{ur0}\left(\sigma_N^u, \varepsilon_N^u, \varepsilon_{LD}^{ur}, S_{LC}^{ur}\right)$ for the hydrostatic, plastic, and compression softening loading curves; $U_{\min}^{Nh}$, $U_{\min}^{Np}$, $U_{\min}^{Ns}$ = nondimensional coefficients determining the minimum unloading tangent stiffness $C_{\min}^{u} = U_{\min}\left(\phi^{ur}, S_{LC}^{ur}\right) \cdot C_N^{ur0}\left(\sigma_N^u, \varepsilon_N^u, \varepsilon_{LD}^{ur}, S_{LC}^{ur}\right)$ for the hydrostatic, plastic, and compression softening loading curves; $R_{\max}^{Nh}$, $R_{\max}^{Np}$, $R_{\max}^{Ns}$ = nondimensional coefficients determining the maximum reloading tangent stiffness $C_{\max}^{r} = R_{\max}\left(\phi^{ur}, S_{LC}^{ur}\right) \cdot C_N^{ur0}\left(\sigma_N^u, \varepsilon_N^u, \varepsilon_{LD}^{ur}, S_{LC}^{ur}\right)$ for the hydrostatic, plastic, and compression softening loading curves; $R_{\min}^{Nh}$, $R_{\min}^{Np}$, $R_{\min}^{Ns}$ = nondimensional coefficients determining the minimum reloading tangent stiffness $C_{\min}^{r} = R_{\min}\left(\phi^{ur}, S_{LC}^{ur}\right) \cdot C_N^{ur0}\left(\sigma_N^u, \varepsilon_N^u, \varepsilon_{LD}^{ur}, S_{LC}^{ur}\right)$ for the hydrostatic, plastic, and compression softening loading curves; ϕ^{ur} = the hardening-softening function for unloading and reloading ($\phi(\varepsilon_{LD})$ value corresponding to the start of unloading in normal compression); $\phi^{ur} = \phi\left(\varepsilon_{LD}^{ur}\right)$; and S_{LC}^{ur} = the lateral confinement stress for unloading and reloading (S_{LC} value corresponding to the start of unloading in normal compression).

The unloading tangent stiffness $C_N^u(\sigma_N)$ and the reloading tangent stiffness $C_N^r(\sigma_N)$ for normal compression are (**Fig.17**)

$$\begin{aligned} C_N^u(\sigma_N) = \Big\{ & \left[U_{\min}\left(\phi^{ur}, S_{LC}^{ur}\right) - U_{\max}\left(\phi^{ur}, S_{LC}^{ur}\right)\right] F^{ur}(\sigma_N) \\ & + U_{\max}\left(\phi^{ur}, S_{LC}^{ur}\right)\Big\} C_N^{ur0}\left(\sigma_N^u, \varepsilon_N^u, \varepsilon_{LD}^{ur}, S_{LC}^{ur}\right) \end{aligned} \tag{51a}$$

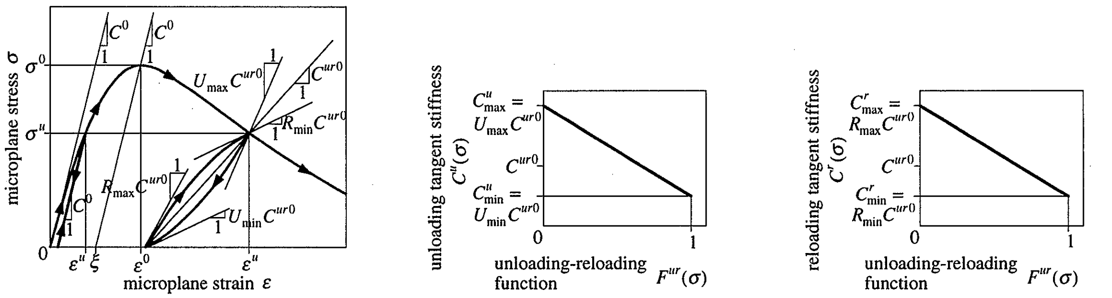

(a) Unloading and reloading for softening loading curve (b) Unloading tangent stiffness (c) Reloading tangent stiffness

Fig.17 Hysteresis rule for a microplane

$$C_N^r(\sigma_N)=\Big\{\big[R_{\min}(\phi^{ur},S_{LC}^{ur})-R_{\max}(\phi^{ur},S_{LC}^{ur})\big]F^{ur}(\sigma_N)$$
$$+R_{\max}(\phi^{ur},S_{LC}^{ur})\Big\}C_N^{ur0}(\sigma_N^u,\varepsilon_N^u,\varepsilon_{LD}^{ur},S_{LC}^{ur}) \tag{51b}$$

On the other hand, in the case of the unloading tangent stiffness $C_N^u(\sigma_N)$ and the reloading tangent stiffness $C_N^r(\sigma_N)$ for normal tension, the lateral strain and stress effects are not taken into account:

$$C_N^u(\sigma_N)=\Big\{\big[U_{\min}^{NT}-U_{\max}^{NT}\big]F^{ur}(\sigma_N)+U_{\max}^{NT}\Big\}C_{NT}^{ur0}(\sigma_N^u,\varepsilon_N^u) \tag{52a}$$

$$C_N^r(\sigma_N)=\Big\{\big[R_{\min}^{NT}-R_{\max}^{NT}\big]F^{ur}(\sigma_N)+R_{\max}^{NT}\Big\}C_{NT}^{ur0}(\sigma_N^u,\varepsilon_N^u) \tag{52b}$$

in which $U_{\max}^{NT}$ = nondimensional coefficient determining the maximum unloading tangent stiffness $C_{\max}^u = U_{\max}^{NT}\cdot C_{NT}^{ur0}(\sigma_N^u,\varepsilon_N^u)$ for the softening loading curve for normal tension; $U_{\min}^{NT}$ = nondimensional coefficient determining the minimum unloading tangent stiffness $C_{\min}^u = U_{\min}^{NT}\cdot C_{NT}^{ur0}(\sigma_N^u,\varepsilon_N^u)$ for the softening loading curve for normal tension; $R_{\max}^{NT}$ = nondimensional coefficient determining the maximum reloading tangent stiffness $C_{\max}^r = R_{\max}^{NT}\cdot C_{NT}^{ur0}(\sigma_N^u,\varepsilon_N^u)$ for the softening loading curve for normal tension; and $R_{\min}^{NT}$ = nondimensional coefficient determining the minimum reloading tangent stiffness $C_{\min}^r = R_{\min}^{NT}\cdot C_{NT}^{ur0}(\sigma_N^u,\varepsilon_N^u)$ for the softening loading curve for normal tension.

It has been confirmed experimentally (for example [18]) that hysteresis loops of concrete during unloading and reloading are very narrow when the concrete is perfectly plastic or under hydrostatic compression. To simulate the macroscopic hysteresis characteristics, linear behavior is assumed during unloading and reloading for the hydrostatic and plastic loading curves of the normal component ignoring hysteresis. On the other hand, hysteresis is assumed during unloading and reloading for the compression softening loading curve after the peak stress, i.e., $\varepsilon_{NC}^u < \varepsilon_{NC}^0$. Also for post-peak tensile region of the normal component, i.e., $\varepsilon_{NT}^u > \varepsilon_{NT}^0$, hysteresis is considered.

Fig.18 shows unloading and reloading responses for normal compression, as calculated with the model described above. These represent the lateral strain and stress effects on the hysteresis response for normal compression. There is no hysteresis in unloading and reloading for the hydrostatic and plastic loading curves. On the other hand, between the plastic loading curve and the compression softening loading curve, hysteresis loops become wider when the virgin loading response, from which unloading starts, approaches the compression softening loading curve, i.e., when S_{LC}^{ur}/S_{LC}^p decreases.

c) Hysteresis Rule for Shear Components

The transition model from brittle to ductile fracture (resolved normal stress dependence) is adopted to calculate hysteresis for microplane shear components. To this end, as with the microplane normal component, nondimensional coefficients $U_{\max}$, $U_{\min}$, $R_{\max}$, and $R_{\min}$ are defined separately for unloading from, and for reloading to, the plastic and softening loading curves of the microplane shear

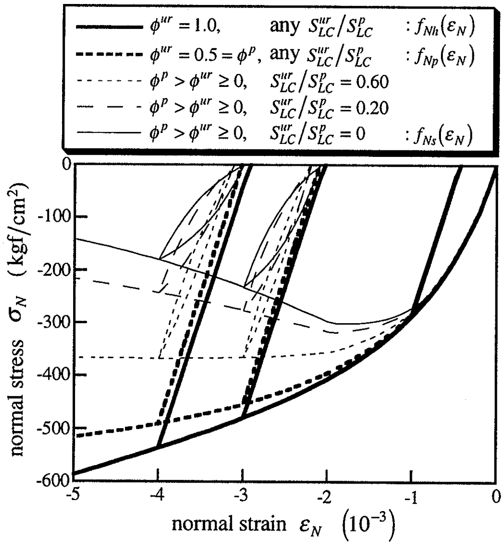

Fig.18 Unloading and reloading responses for normal compression

component. Weighting those coefficients, the coefficients corresponding to the resolved normal stress S_N^{ur} for unloading and reloading are calculated using a method similar to the virgin loading curve described in **3.5 a)** .

When $S_N^{ur} \leq S_N^{p}$:

$$U_{\max}\left(S_N^{ur}\right) = U_{\max}^{Tp} \tag{53a}$$

$$U_{\min}\left(S_N^{ur}\right) = U_{\min}^{Tp} \tag{53b}$$

$$R_{\max}\left(S_N^{ur}\right) = R_{\max}^{Tp} \tag{53c}$$

$$R_{\min}\left(S_N^{ur}\right) = R_{\min}^{Tp} \tag{53d}$$

when $S_N^{p} < S_N^{ur} < 0$:

$$U_{\max}\left(S_N^{ur}\right) = \left(\frac{S_N^{ur}}{S_N^{p}}\right)U_{\max}^{Tp} + \left(\frac{S_N^{p} - S_N^{ur}}{S_N^{p}}\right)U_{\max}^{TC} \tag{53e}$$

$$U_{\min}\left(S_N^{ur}\right) = \left(\frac{S_N^{ur}}{S_N^{p}}\right)U_{\min}^{Tp} + \left(\frac{S_N^{p} - S_N^{ur}}{S_N^{p}}\right)U_{\min}^{TC} \tag{53f}$$

$$R_{\max}\left(S_N^{ur}\right) = \left(\frac{S_N^{ur}}{S_N^{p}}\right)R_{\max}^{Tp} + \left(\frac{S_N^{p} - S_N^{ur}}{S_N^{p}}\right)R_{\max}^{TC} \tag{53g}$$

$$R_{\min}\left(S_N^{ur}\right) = \left(\frac{S_N^{ur}}{S_N^{p}}\right)R_{\min}^{Tp} + \left(\frac{S_N^{p} - S_N^{ur}}{S_N^{p}}\right)R_{\min}^{TC} \tag{53h}$$

when $0 \leq S_N^{ur}$:

$$U_{\max}\left(S_N^{ur}\right) = U_{\max}^{TT} \tag{53i}$$

$$U_{\min}\left(S_N^{ur}\right) = U_{\min}^{TT} \tag{53j}$$

$$R_{\max}\left(S_N^{ur}\right) = R_{\max}^{TT} \tag{53k}$$

$$R_{\min}\left(S_N^{ur}\right) = R_{\min}^{TT} \tag{53l}$$

in which $U_{\max}^{Tp}$, $U_{\max}^{TC}$, $U_{\max}^{TT}$ = nondimensional coefficients determining the maximum unloading tangent stiffness $C_{\max}^{u} = U_{\max}\left(S_N^{ur}\right) \cdot C_T^{ur0}\left(\sigma_T^{u}, \varepsilon_T^{u}, S_N^{ur}\right)$ for the plastic loading curve and softening loading curves

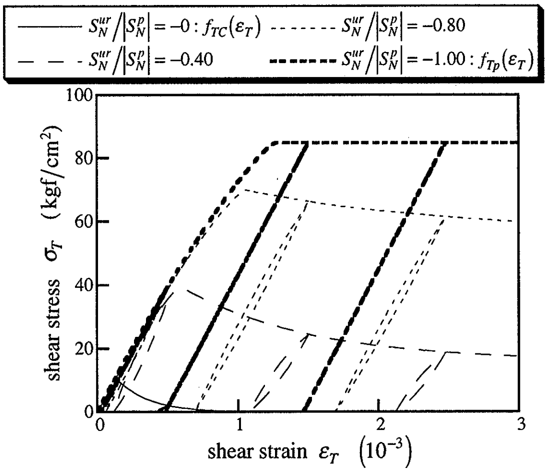

Fig.19 Unloading and reloading responses for tension of shear

under resolved normal compression and tension stresses; $U_{\min}^{Tp}$, $U_{\min}^{TC}$, $U_{\min}^{TT}$ = nondimensional coefficients determining the minimum unloading tangent stiffness $C_{\min}^{u} = U_{\min}(S_N^{ur}) \cdot C_T^{ur0}(\sigma_T^u, \varepsilon_T^u, S_N^{ur})$ for the plastic loading curve and softening loading curves under resolved normal compression and tension stresses; $R_{\max}^{Tp}$, $R_{\max}^{TC}$, $R_{\max}^{TT}$ = nondimensional coefficients determining the maximum reloading tangent stiffness $C_{\max}^{r} = R_{\max}(S_N^{ur}) \cdot C_T^{ur0}(\sigma_T^u, \varepsilon_T^u, S_N^{ur})$ for the plastic loading curve and softening loading curves under resolved normal compression and tension stresses; and $R_{\min}^{Tp}$, $R_{\min}^{TC}$, $R_{\min}^{TT}$ = nondimensional coefficients determining the minimum reloading tangent stiffness $C_{\min}^{r} = R_{\min}(S_N^{ur}) \cdot C_T^{ur0}(\sigma_T^u, \varepsilon_T^u, S_N^{ur})$ for the plastic loading curve and softening loading curves under resolved normal compression and tension stresses.

The unloading tangent stiffness $C_T^u(\sigma_T)$ and the reloading tangent stiffness $C_T^r(\sigma_T)$ for the shear component are

$$C_T^u(\sigma_T) = \left\{ \left[U_{\min}(S_N^{ur}) - U_{\max}(S_N^{ur}) \right] F^{ur}(\sigma_T) + U_{\max}(S_N^{ur}) \right\} C_T^{ur0}(\sigma_T^u, \varepsilon_T^u, S_N^{ur}) \tag{54a}$$

$$C_T^r(\sigma_T) = \left\{ \left[R_{\min}(S_N^{ur}) - R_{\max}(S_N^{ur}) \right] F^{ur}(\sigma_T) + R_{\max}(S_N^{ur}) \right\} C_T^{ur0}(\sigma_T^u, \varepsilon_T^u, S_N^{ur}) \tag{54b}$$

Hysteresis is assumed during unloading and reloading for the softening loading curves under resolved normal compression and tension stresses after the peak stress, i.e., $|\varepsilon_{TC}^0| < |\varepsilon_T^u|$ and $|\varepsilon_{TT}^0| < |\varepsilon_T^u|$. On the other hand, linear behavior is assumed during unloading and reloading for the plastic loading curve of the shear component ignoring hysteresis.

Fig.19 shows unloading and reloading responses for tension of shear, as calculated using this model, representing the transition model from brittle to ductile fracture (resolved normal stress dependence) for microplane shear hysteresis. There is no hysteresis in unloading and reloading for the plastic loading curve. On the other hand, between the plastic loading curve and the softening loading curve, hysteresis loops become wider when the virgin loading response, from which unloading starts, approaches the softening loading curve, i.e., when $S_N^{ur}/|S_N^p|$ increases.

3.8 Alternating Cyclic Loading Rule for Microconstitutive Relations

The foregoing rules apply separately to the tension and compression regions of each microplane component. The borderline between the tension and compression regions is defined by zero microplane stress. To establish a complete cyclic loading model for the microplane, the foregoing rule must be

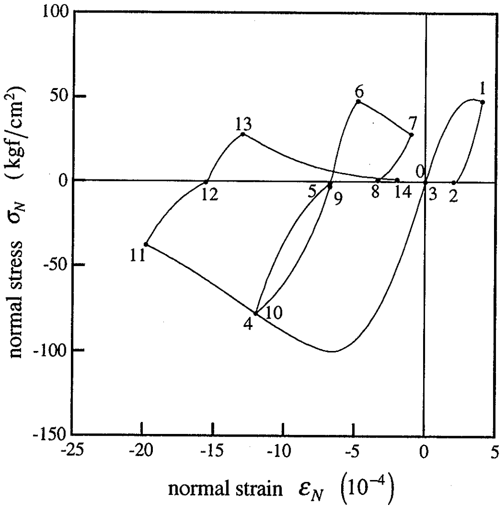

Fig.20 Cyclic response for normal component

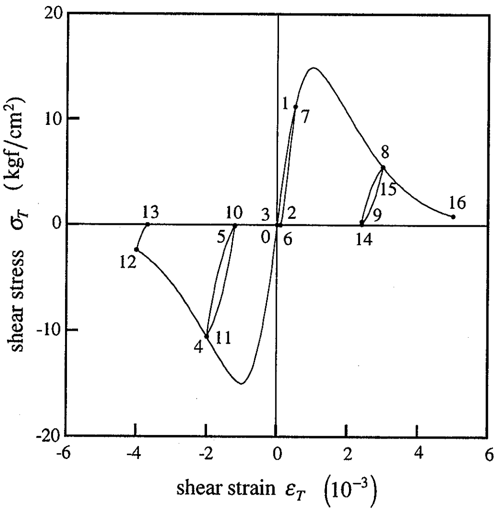

Fig.21 Cyclic response for shear component

extended to cover the entire range of tensile and compressive microplane stresses. To identify the alternating cyclic loading rule for each microplane component, many possible cases of the cyclic rule were tried numerically and compared to uniaxial compressive and tensile tests in the literature.

The alternating cyclic loading rule for the normal component is characterized as follows.
1) The virgin stress-strain curves for both normal tension and compression are unique regardless of the number of cycles or the strain history.
2) The origin of the virgin stress-strain curve for normal compression is fixed. However, the one for normal tension can shift along the strain axis when unloading in the compression region goes into the tension region.
3) When unloading in the compression region goes further into the tension region, loading or reloading in the tension region starts from the plastic residual strain for the compression region.
4) When unloading in the tension region goes further into the compression region, there is a horizontal plateau with zero normal stress before loading or reloading in the compression region starts at the plastic residual strain for the previous compression unloading.

Fig.20 is an example of a calculated cyclic response using the alternating cyclic loading rule for the normal component with the compression softening loading curve. In this figure, the normal strain history is marked with sequential numbers. In this example, the first cycle enters tensile softening, and then reverts to compression. Before going into compressive stress, there is a plateau which corresponds to closing of microcracks. The compression region begins always at the origin (zero normal strain), but the origin of tension is shifted every time unloading from the compression region crosses the strain axis.

The alternating cyclic loading rule for the shear component is characterized as follows.
1) The virgin stress-strain curves for both tension and compression of shear are unique regardless of the number of cycles or the strain history.
2) The origins of virgin stress-strain curves for tension and compression of shear are fixed.
3) When unloading in one region goes further into another region, there is a horizontal plateau with zero shear stress before loading or reloading in the latter region starts at the plastic residual strain for the previous unloading.

Fig.21 is an example of a calculated cyclic response using the alternating cyclic loading rule for the shear component, in which the shear strain history is marked with sequential numbers. The origins of the stress-strain curves for both tension and compression regions are fixed. In the example shown, the strain cycles are similar to those used in the previous example for the normal component, but the stress responses are very different. After the unloading curves reach the strain axis, there are always plateaus of zero shear stress. This assumption is needed to model experimental observations showing that for large deformations almost no stress change occurs in crack shear (aggregate interlock) tests with stress reversals. Such behavior is due to free play between asperities or between the faces of opened cracks which need to come into contact before the stress can reverse its sign.

4. VERIFICATION OF ENHANCED MICROPLANE CONCRETE MODEL

In this third part of the present study, the Enhanced Microplane Concrete Model is verified by comparing calculated results using the model with experimentally obtained constitutive relations for concrete as reported in the literature for various stress conditions. Examination of the microplane responses in each analysis provides an explanation of the load-carrying mechanisms in concrete in terms of responses on the microplanes.

4.1 Verification Analysis

To verify the general applicability of the Enhanced Microplane Concrete Model, constitutive relations covering a wide range of stress conditions are simulated with a single set of input material parameters for the model. Several series of analyses were carried out [7], from which the following two series, B1 and B2, are reported here:

1) Analysis series B1

The triaxial compressive tests along the compressive meridian carried out by Smith et al. [8] are first simulated, and then triaxial compressive analysis along the tensile meridian, biaxial compression analysis, biaxial compression-tension analysis, and biaxial tension analysis are done with the identical input material parameters to simulate the tests.

2) Analysis series B2

Cyclic responses under uniaxial, biaxial, and triaxial compression are calculated and compared with the experiments by van Mier [19]. Extracting invariants of stress and strain tensors from the obtained analytical responses, the relations between the invariants are compared with the corresponding experiments.

The constitutive equations (14) are solved with boundary conditions for each analysis. As with the previous calculations, integrations in the equations are evaluated using the numerical integration formula derived by Bazant and Oh [9].

4.2 Material Parameters

In the Enhanced Microplane Concrete Model, there are three groups of material parameters except for Young's modulus E^0 and Poisson's ratio ν^0:

1) material parameters concerning virgin loading for the microplane,
2) material parameters concerning unloading and reloading for the microplane,
3) material parameters concerning rate effects for the microplane.

Table 3 shows the material parameters in groups 1) and 3) as used in analysis series B1 and B2.

For the hydrostatic loading curve of the normal component, the material parameters previously identified for the experiment by Green and Swanson are utilized. Since the present analysis is intended for a single static strain rate, we eliminate the strain rate effect by specifying infinite values of relaxation time ρ^∞. The relaxation times shown in **Table 3** are the assumed infinite values.

For the material parameters concerning unloading and reloading for the microplane, the following values are assumed:

$$\alpha_{NT} = \alpha_{NC} = \alpha_{TT} = \alpha_{TC} = 0.2 \tag{55}$$

$$U_{\max}^{NT} = U_{\max}^{Ns} = U_{\max}^{TT} = U_{\max}^{TC} = 2.0 \tag{56a}$$

$$U_{\min}^{NT} = U_{\min}^{Ns} = U_{\min}^{TT} = U_{\min}^{TC} = 0.5 \tag{56b}$$

$$R_{\max}^{NT} = R_{\max}^{Ns} = R_{\max}^{TT} = R_{\max}^{TC} = 2.0 \tag{56c}$$

$$R_{\min}^{NT} = R_{\min}^{Ns} = R_{\min}^{TT} = R_{\min}^{TC} = 0.5 \tag{56d}$$

Table 3 Material parameters for Enhanced Microplane Concrete Model

material parameter		analysis series B1	B2 uniaxial	B2 biaxial	B2 triaxial	recommen-dation
normal tension	σ_{NT}^0 (kgf/cm^2)	40.0	45.0	45.0	50.0	$(1.2 \sim 1.3)f_t$
	ζ_{NT}	0.5	0.5	0.5	0.5	0.5
	γ_{NT}	5.0	5.0	5.0	5.0	5.0
	p_{NT}	1.0	1.0	1.0	1.0	1.0
	ρ_{NT} (sec)	10^5	10^5	10^5	10^5	10^5
normal compression (softening)	σ_{NC}^0 (kgf/cm^2)	-400	-600	-600	-500	$(1.2 \sim 1.4)f_c$
	ζ_{NC}	0.3	0.7	0.7	0.3	0.3
	γ_{NC}	1.0	1.0	1.0	0.5	1.0
	p_{NC}	1.0	1.0	1.0	1.0	1.0
	ρ_{NC} (sec)	10^7	10^7	10^7	10^7	10^7
normal compression (plasticity)	σ_{Np}^0 (kgf/cm^2)	-1200	-1200	-1200	-1200	$(3.0 \sim 4.0)f_c$
	ζ_{Np}	0.3	0.3	0.3	0.3	0.3
shear (tensile S_N)	σ_{TT}^0 (kgf/cm^2)	17.0	30.0	30.0	20.0	$(0.5 \sim 0.8)f_t$
	ζ_{TT}	0.9	0.9	0.9	0.9	0.9
	γ_{TT}	0.5	0.5	0.5	0.5	0.5
	p_{TT}	1.0	1.0	1.0	1.0	1.0
	μ_{TT}	4.0	4.0	4.0	4.0	4.0
	$r_{\min}^0$	0.1	0.1	0.1	0.1	0.1
	ρ_{TT} (sec)	10^6	10^6	10^6	10^6	10^6
shear (compressive S_N)	σ_{TC}^0 (kgf/cm^2)	17.0	30.0	30.0	20.0	$(0.5 \sim 0.8)f_t$
	ζ_{TC}	0.5	0.7	0.9	0.5	0.7
	γ_{TC}	1.0	1.0	1.0	1.0	1.0
	p_{TC}	1.0	1.0	1.0	1.0	1.0
	μ_{TC}	0.6	0.6	0.6	0.6	0.6
	S_N^p (kgf/cm^2)	-300	-600	-400	-400	$(0.8 \sim 1.0)f_c$
	ρ_{TC} (sec)	10^6	10^6	10^6	10^6	10^6
lateral effects	ε_{LD}^1	0.003	0.003	0.003	0.003	0.003
	ε_{LD}^p	0.003	0.003	0.003	0.003	0.003
	m	1.0	1.0	1.0	1.0	1.0
	S_{LC}^p (kgf/cm^2)	-500	-300	-300	-300	$(0.7 \sim 1.6)f_c$
analytical results	f_c' (kgf/cm^2)	336	439	454	417	
	f_t (kgf/cm^2)	30.1	37.1	35.8	38.4	
experimental results	f_c' (kgf/cm^2)	343	429	492	434	
	f_t (kgf/cm^2)	—	28.1	28.5	28.1	

(shaded) : fixed constant

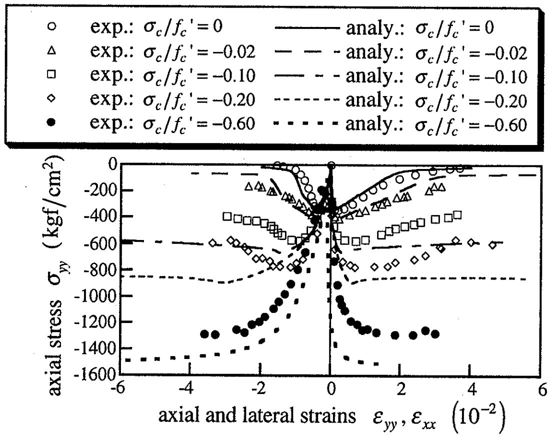

Fig.22 Triaxial compression analysis along compressive meridian using Enhanced Microplane Concrete Model

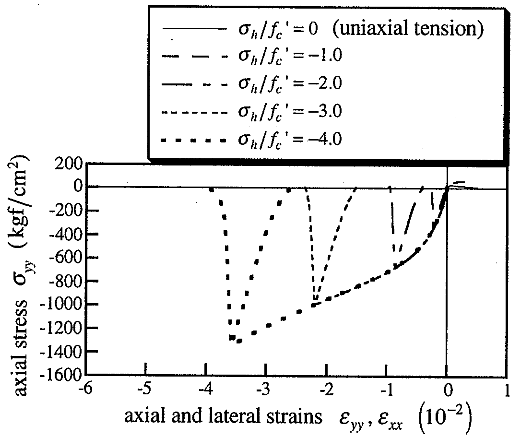

Fig.23 Triaxial compression analysis along tensile meridian using Enhanced Microplane Concrete Model

$$U_{\max}^{Np} = U_{\min}^{Np} = R_{\max}^{Np} = R_{\min}^{Np} = 1.0 \tag{56e}$$
$$U_{\max}^{Nh} = U_{\min}^{Nh} = R_{\max}^{Nh} = R_{\min}^{Nh} = 1.0 \tag{56f}$$
$$U_{\max}^{Tp} = U_{\min}^{Tp} = R_{\max}^{Tp} = R_{\min}^{Tp} = 1.0 \tag{56g}$$

As shown in **Table 3** twenty-one parameters are fixed constant in the analysis. Some of the other parameters have strong correlations with the uniaxial compressive strength f_c' or uniaxial tensile strength f_t. Recommended values for the material parameters taking this into account are given in **Table 3**.

4.3 Triaxial Compression Analysis (Analysis Series B1)

Fig.22 shows the result of triaxial compression analysis along the compressive meridian in comparison with the experiments by Smith et al., in which σ_c = confinement pressure; and f_c' = uniaxial compressive strength. The model predicts increases in strength and ductility with confinement pressure

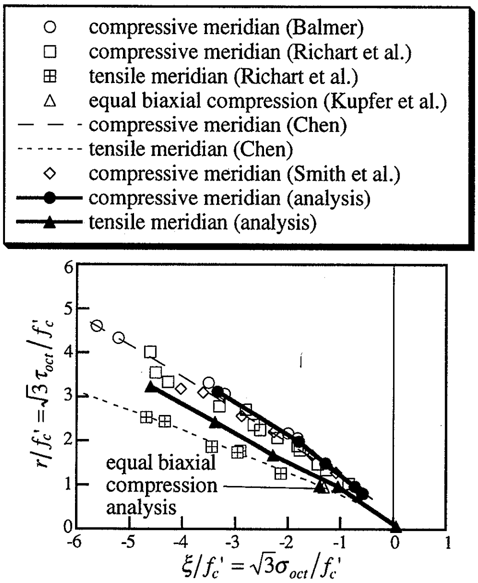

Fig.24 Compressive and tensile meridians for Enhanced Microplane Concrete Model

under triaxial compression with practical accuracy, i.e., the transition from brittle to ductile fracture. This is due to rational modeling of responses on the microplane. In **Fig.23**, calculated triaxial compression responses along the tensile meridian are shown, in which σ_h is the hydrostatic pressure. The compressive and tensile meridians of the failure envelope are evaluated from maximum stresses obtained in the analyses, and shown in **Fig.24** with experimental results from the literature (Balmer [10], Richart et al. [11], Kupfer et al. [12], Smith et al. [8], and Chen [13]), where $\sigma_{oct} = I_1/3 = \sigma_{ii}/3$ and $\tau_{oct} = \sqrt{2J_2/3}$ are octahedral normal and shear stresses (J_2 = the 2nd invariant of deviatoric stress tensor). The model predicts the compressive meridian very well, but it slightly overestimates the tensile meridian.

Figs.25 and **26** show the normal, K-shear, and M-shear responses of microplanes (integration points) 2, 3, and 14 as well as the average volumetric responses ε_{av} for the uniaxial $(\sigma_c/f_c' = 0)$ and triaxial $(\sigma_c/f_c' = -0.60)$ compression analyses. We can see from **Fig.25(b)** that normal tension damage of microplane 3, representing splitting cracks under lower macroscopic compressive stress, causes macroscopic strength reduction in the uniaxial compression analysis. On the other hand, normal compression stress occurring on microplane 3 when macroscopic confinement pressure is applied delays normal tension damage as if it were a prestress, resulting in a macroscopic strength increase for the triaxial compression analysis (**Fig.26(b)**). In uniaxial compression experiments [20], [21], [22] microcracks occur at the interface region (corresponding to microplane 3) between the coarse aggregate particles and the mortar matrix parallel to the loading direction at the earlier loading stage, and at the final loading stage the failure is completed by fracture of the interface region (corresponding to microplane 2) normal to the loading direction. This is consistent with the analytical results on microplane response. In the triaxial compression experiments by Krishnaswamy [23] and Niwa et al. [24], an increase in confinement pressure delays interfacial microcracking between the coarse aggregate particles and the mortar matrix, and suppresses prominent mortar cracks. This is consistent with the mechanism of the confinement effect in the analysis.

Since the lateral strain and stress effects for the normal component as well as the transition model from brittle to ductile fracture with confinement for the shear component are taken into account in the Enhanced Microplane Concrete Model, the normal compression and shear responses at microplanes 2 and 14 shown in **Figs.26(a)** and **(c)** exhibit plastic flows in the triaxial compression analysis. These microplane responses result in the macroscopic confinement effect with practical accuracy. On the other hand, it has been shown that with the previous Microplane Concrete Model all microplanes ultimately exhibit strain-softening responses, which resulted in insufficient confinement effect.

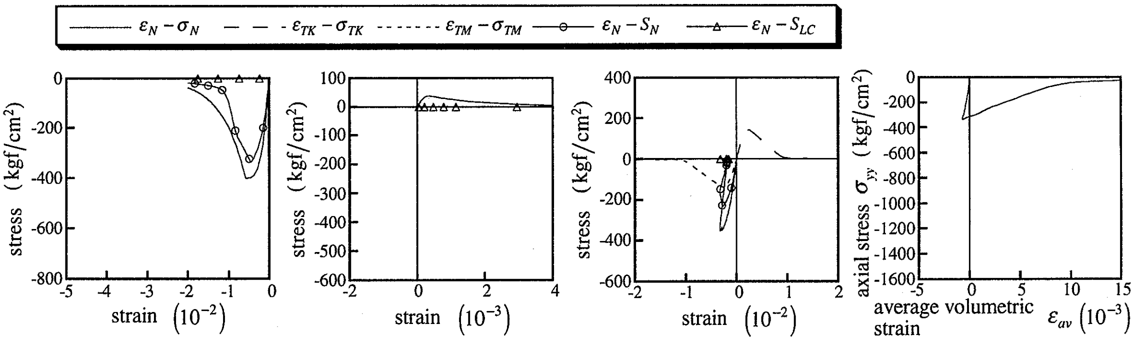

(a) Microplane 2 (b) Microplane 3 (c) Microplane 14 (d) Average volumetric response

Fig.25 Responses in uniaxial compression analysis using Enhanced Microplane Concrete Model

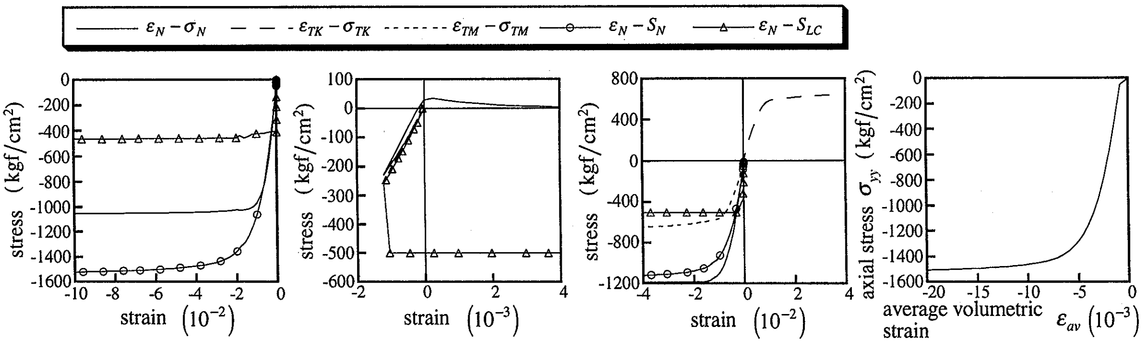

(a) Microplane 2 (b) Microplane 3 (c) Microplane 14 (d) Average volumetric response

Fig.26 Responses in triaxial compression analysis $(\sigma_c/f_c' = -0.60)$ using Enhanced Microplane Concrete Model

In **Figs.25(a) - (c)** and **Figs.26(a) - (c)** histories of resolved normal stress S_N and lateral confinement stress S_{LC} are shown with normal strain on each microplane. The S_N and S_{LC} values in the uniaxial compression analysis are much smaller than those in the triaxial compression analysis. Therefore, the normal and shear responses in the uniaxial compression analysis exhibit softening with lower peak stresses, which results in brittle uniaxial compression behavior and lower macroscopic peak stress as compared with the triaxial compression.

As shown in **Fig.25(c)** unloading in the normal compression response at microplane 14 starts approximately when the macroscopic peak stress is reached, since the normal strain increment at microplane 14 changes from a compressive value to a tensile one due to the macroscopic volumetric dilatancy at the peak stress (**Fig.25(d)**). The unloading response is considered an important microscopic mechanism with which the present model can offer path dependence. In uniaxial compression experiments [20], [21], [22] similar unloading responses were microscopically observed at an inclined orientation to the loading axis, which is consistent with this analysis.

4.4 Biaxial Analysis (Analysis Series B1)

In **Figs.27** and **28** the results of biaxial compression and compression-tension analyses are compared with experiments reported by Kupfer et al. [12]. Negative values of ε_{c0} in these figures represent axial strains corresponding to the uniaxial compressive strength f_c'. The stress-strain responses under biaxial tension as well as uniaxial tension are shown in **Fig.29**. Relatively good agreement between calculation and experiment is achieved for all stress conditions. Especially constitutive relations under

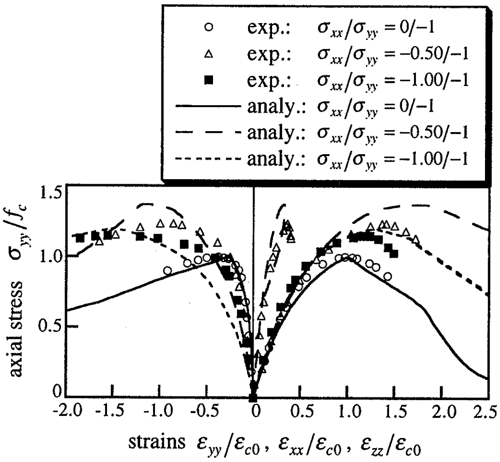

Fig.27 Biaxial compression analysis using Enhanced Microplane Concrete Model

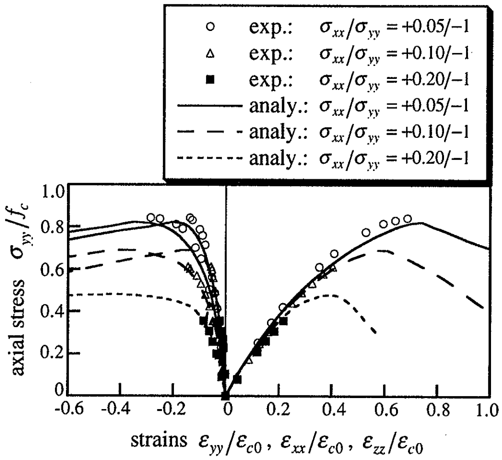

Fig.28 Biaxial compression-tension analysis using Enhanced Microplane Concrete Model

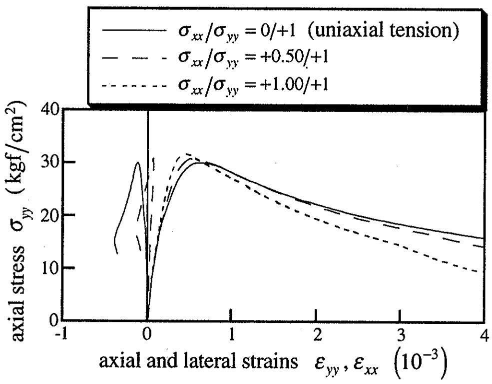

Fig.29 Biaxial tension analysis using Enhanced Microplane Concrete Model

biaxial compression are well predicted by the model not only for the hardening regime but also for the strain-softening regime. The stress-strain relations as well as peak stresses under biaxial tension are little different from those under uniaxial tension in the analysis, which represents a characteristic of concrete materials.

The analytical responses under biaxial tension exhibit considerable nonlinearity in the pre-peak regime, while typical average stress-strain relations in the experiments show almost perfect elasticity under biaxial tension. This model is thought to be capable of evaluating nonlinear behavior in a highly localized damage region such as a fracture process zone. In the uniaxial tension analysis, the apparent Poisson's ratio, defined as the ratio of total lateral strain to total tensile axial strain, is always positive, thus verifying the rationality of the present model as a tensile constitutive law. On the other hand, as described before, the volumetric-deviatoric-shear component formulation predicts lateral expansion with a negative Poisson's ratio in the uniaxial tension analysis, which is unacceptable for concrete.

Fig.30 shows the analytical result for the biaxial strength envelope compared with experiments by Kupfer et al. [12]. It confirms that the biaxial strength of concrete can be estimated with accuracy using the present model. The obtained ratio of uniaxial tensile strength to uniaxial compressive strength in the analysis agrees well with typical experimental values.

Fig.31 shows the normal, K-shear, and M-shear responses of microplanes (integration points) 2, 3, and 14 as well as the average volumetric response ε_{av} for the uniaxial tension analysis. Since the concept of shear frictional coefficient is applied not only to negative values of resolved normal stress S_N but

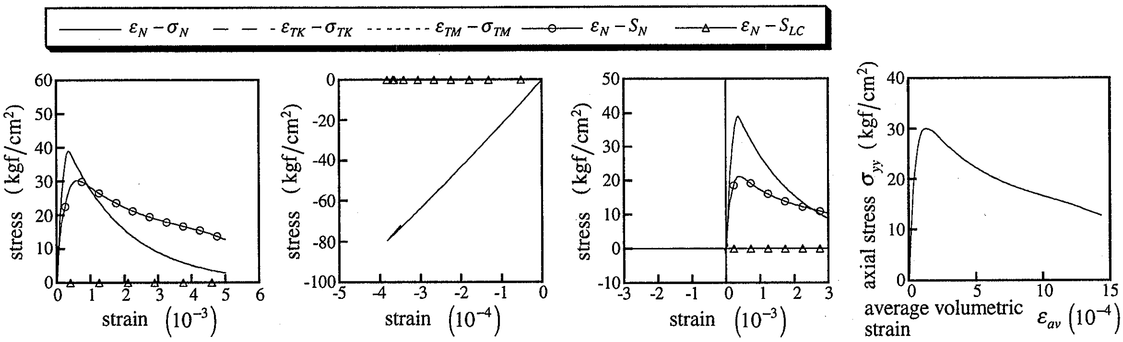

(a) Microplane 2 (b) Microplane 3 (c) Microplane 14 (d) Average volumetric response

Fig.31 Responses in uniaxial tension analysis using Enhanced Microplane Concrete Model

also to positive ones as in (43), the shear peak stresses on microplane 14, where the resolved normal stress has a large, tensile value, are small, and the shear components lose their load-carrying capacity at an earlier stage of the uniaxial tension analysis (**Fig.31(c)**); the peak stresses of K-shear and M-shear are -1.9 and $+2.3$ $\mathrm{kgf/cm^2}$, respectively. On the other hand, normal tensile damage on the microplanes is prominent compared with the shear damage. These analytical results suggest that tensile (Mode I) microcracks dominate the macroscopic fracture of concrete under tension, although shear (Mode II) microcracks occur simultaneously. This is consistent with experimental observations of the microscopic fracture mechanism using acoustic emission techniques [25].

4.5 Cyclic Loading Analysis (Analysis Series B2)

a) Cyclic Uniaxial Compressive Behavior

In **Fig.32** calculated cyclic response under uniaxial compression is compared with the experiment by van Mier [19], in which the lower limit value $\sigma_{\lim}$ of variable stress amplitude was $-50\,\mathrm{kgf/cm^2}$. A similar analysis with $\sigma_{\lim} = 0\,\mathrm{kgf/cm^2}$ is carried out, and the result is shown in the same figure. **Fig.33** shows the normal, K-shear, and M-shear responses of microplanes (integration points) 2, 3, and 14 as well as the average volumetric response ε_{av} for the uniaxial compression analysis with $\sigma_{\lim} = 0\,\mathrm{kgf/cm^2}$.

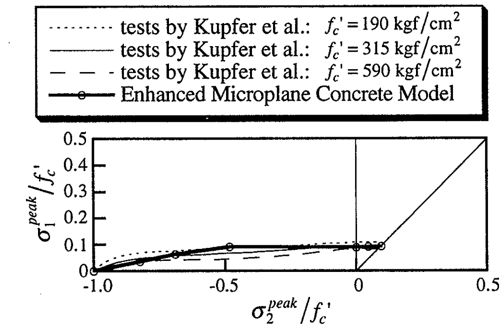

(a) Compression-tension and tension-tension stress regions

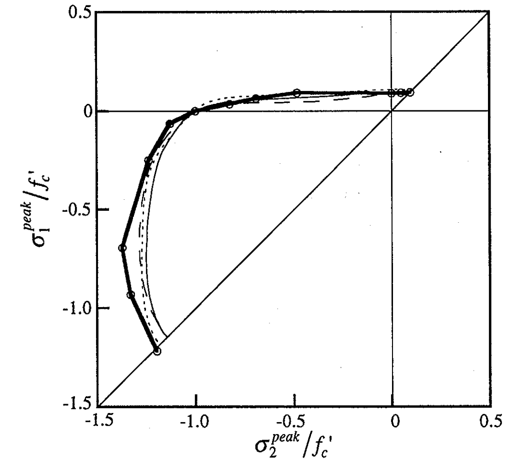

(b) Entire region of biaxial stress

Fig.30 Biaxial strength envelopes

Although the degradation of unloading and reloading stiffnesses in the experiment are well predicted by the model, as shown in **Fig.32**, the analysis underestimates strain-softening stiffness and lateral strain in softening regime as compared with the experiment. The present analysis assumes a uniform stress and strain state for the specimen, and neglects localization of strain softening and fracture, and this is one of the causes for the underestimated lateral strain.

The change in shape and width of hysteresis loops during uniaxial compressive loading of concrete is

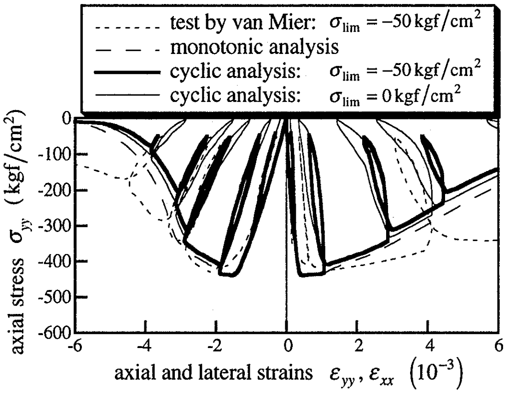

Fig.32 Cyclic uniaxial compression analysis using Enhanced Microplane Concrete Model

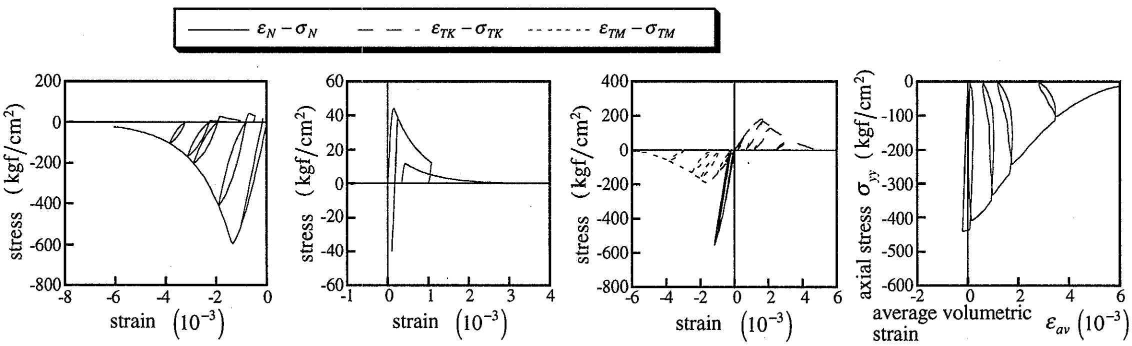

(a) Microplane 2 (b) Microplane 3 (c) Microplane 14 (d) Average volumetric response

Fig.33 Responses in cyclic uniaxial compression analysis $(\sigma_{\lim} = 0\,\mathrm{kgf/cm^2})$ using Enhanced Microplane Concrete Model

well captured by the model. Since normal compression unloading proceeds into normal tension softening on microplane 2 in the analysis for $\sigma_{\lim} = 0\,\mathrm{kgf/cm^2}$ (**Fig.33(a)**), curvature of the macroscopic hysteresis loop at lower stress levels becomes prominent.

b) Cyclic Biaxial Compressive Behavior

In **Fig.34** calculated cyclic and monotonic responses under biaxial compression are compared with the experiment by van Mier [19], in which the biaxial stress ratio was $\sigma_{xx}/\sigma_{yy} = -0.05/-1$, and the lower limit value $\sigma_{\lim}$ of variable stress amplitude was $0\,\mathrm{kgf/cm^2}$. **Fig.35** shows the normal, *K*-shear, and *M*-shear responses of microplanes (integration points) 2, 3, and 14 as well as the average volumetric response ε_{av} for the biaxial compression analysis.

The model well describes strain-softening stiffness and the degradation of unloading and reloading stiffnesses during strain softening under biaxial compression; however, lateral strain ε_{xx} is overestimated in the calculation as compared with the experiment.

As with the cyclic uniaxial compression analysis, the curvature of the macroscopic hysteresis loop at lower stress levels under biaxial compression depends on the alternating cyclic loading response when normal compression unloading proceeds into normal tension loading. As shown in **Fig.33(a)**, **(b)** and **Figs.35(a)**, **(b)**, macroscopic tensile strain and cyclic loading cause tensile microplane stress to be induced on microplanes where there is no resolved tensile component of the macroscopic stress tensor. This tensile microplane stress causes microscopic damage, which then results in macroscopic damage and stiffness degradation. In a heterogeneous concrete material with no macroscopic tensile stress, microscopic tensile strain and stress are induced on a microscopic level or meso-level, becoming the

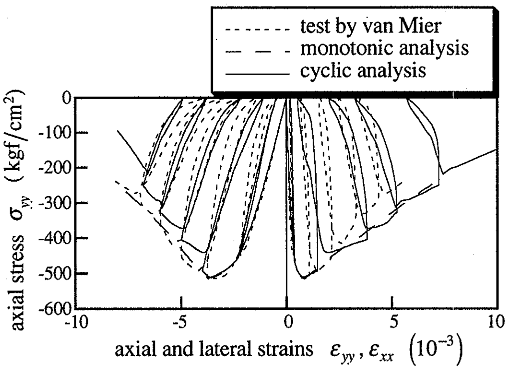

Fig.34 Cyclic biaxial compression analysis using Enhanced Microplane Concrete Model

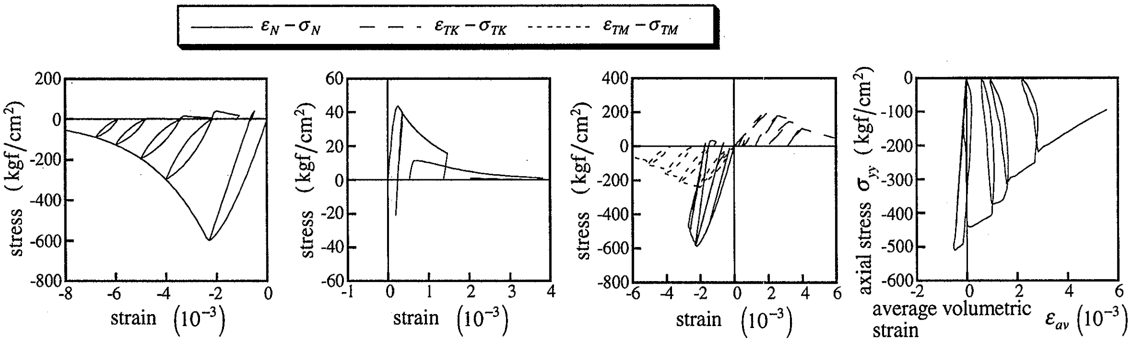

(a) Microplane 2 (b) Microplane 3 (c) Microplane 14 (d) Average volumetric response

Fig.35 Responses in cyclic biaxial compression analysis using Enhanced Microplane Concrete Model

origin of macroscopic damage [20]-[24], [26], [27]. The model accounts for the microscopic damage mechanism in macroscopic constitutive modeling in a simple and reasonable way without a complicated micromechanics model.

c) Cyclic Triaxial Compressive Behavior

In **Fig.36** calculated cyclic and monotonic responses under triaxial compression are compared with the experiment by van Mier [19], in which a confinement pressure of $\sigma_{xx} = \sigma_{zz} = \sigma_c = -10.2\ \mathrm{kgf/cm^2}$ was applied first and held constant, and then compressive axial strain ε_{yy} was applied cyclically with $\sigma_{\lim} = -12.8\ \mathrm{kgf/cm^2}$. **Fig.37** shows the normal, *K*-shear, and *M*-shear responses of microplanes (integration points) 2, 3, and 14 as well as the average volumetric response ε_{av} for the triaxial compression analysis.

The strain-softening stiffness and degradation of unloading and reloading stiffnesses during strain softening under triaxial compression are well captured by the model. However, the width of the hysteresis loops is small and the curvature of the hysteresis loop at lower stress levels is too large in the analysis.

d) Extraction of Invariants

Based on the cyclic uniaxial, biaxial, and triaxial compression analyses, the total strain tensor ε_{ij} is resolved into elastic ε_{eij} and plastic ε_{pij} strain tensors assuming that the residual strain after complete unloading is the plastic strain at the start of unloading σ_{ij}. The following deviatoric tensors are calculated from the stress and strain tensors:

$$s_{ij} = \sigma_{ij} - \frac{1}{3}\sigma_{kk}\delta_{ij} \tag{57}$$

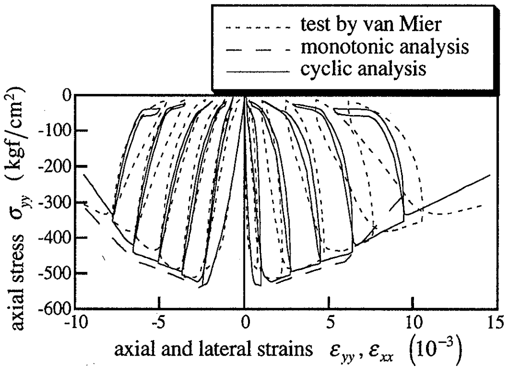

Fig.36 Cyclic triaxial compression analysis using Enhanced Microplane Concrete Model

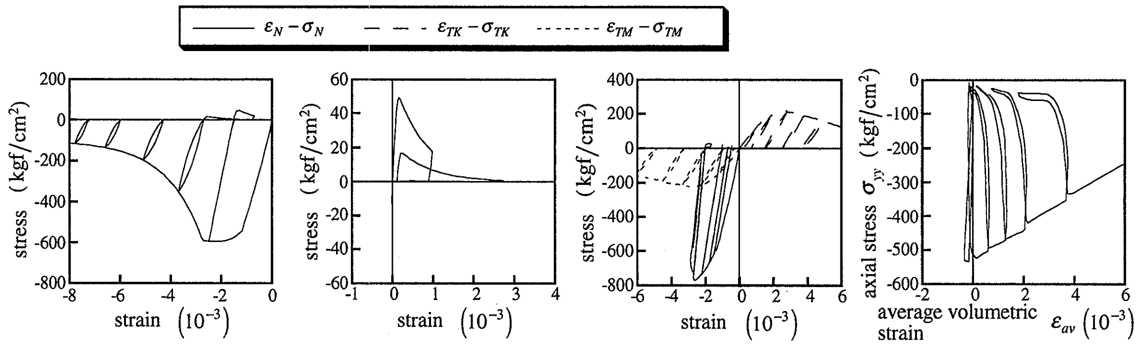

(a) Microplane 2 (b) Microplane 3 (c) Microplane 14 (d) Average volumetric response

Fig.37 Responses in cyclic triaxial compression analysis using Enhanced Microplane Concrete Model

$$e_{ij} = \varepsilon_{ij} - \frac{1}{3}\varepsilon_{kk}\delta_{ij} \tag{58}$$

$$e_{eij} = \varepsilon_{eij} - \frac{1}{3}\varepsilon_{ekk}\delta_{ij} \tag{59}$$

$$e_{pij} = \varepsilon_{pij} - \frac{1}{3}\varepsilon_{pkk}\delta_{ij} \tag{60}$$

in which s_{ij} = deviatoric stress tensor; e_{ij} = deviatoric strain tensor; e_{eij} = elastic deviatoric strain tensor; and e_{pij} = plastic deviatoric strain tensor.

Maekawa et al. [28], [29] extracted several invariants from their experiment and used them to derive an elastoplastic and fracture constitutive model. In this study, the following invariants from their research are chosen and calculated for the cyclic compression analysis described above:

$$I_1^{\text{mod}} = \frac{1}{3}\sigma_{ii} \tag{61}$$

$$J_2^{\text{mod}} = \sqrt{\frac{1}{2}s_{ij}s_{ij}} \tag{62}$$

$$I_{1e}^{\text{mod}} = \frac{1}{3}\varepsilon_{eii} \tag{63}$$

$$J_{2e}^{\text{mod}} = \sqrt{\frac{1}{2}e_{eij}e_{eij}} \tag{64}$$

$$I_{1p}^{\mathrm{mod}} = \frac{1}{3}\varepsilon_{pii} \tag{65}$$

$$J_{2p}^{\mathrm{mod}} = \sqrt{\frac{1}{2}e_{pij}e_{pij}} \tag{66}$$

$$K = \frac{J_2^{\mathrm{mod}}}{2G^0 J_{2e}^{\mathrm{mod}}} \tag{67}$$

in which I_1^{mod} = modified 1st invariant of stress tensor; J_2^{mod} = modified 2nd invariant of deviatoric stress tensor; I_{1e}^{mod} = modified 1st invariant of elastic strain tensor; J_{2e}^{mod} = modified 2nd invariant of elastic deviatoric strain tensor; I_{1p}^{mod} = modified 1st invariant of plastic strain tensor; J_{2p}^{mod} = modified 2nd invariant of plastic deviatoric strain tensor; K = fracture parameter; and G^0 = initial shear modulus, $G^0 = E^0/2(1+\nu^0)$. The superscript 'mod' refers to a modified value because its definition differs slightly from the usual one.

Fig.38(a) shows the $I_{1e}^{\mathrm{mod'}}/\varepsilon_{c0}'$ - $I_1^{\mathrm{mod'}}/f_c'$ relation calculated from the results of the present cyclic compression analysis as compared with that calculated for the experiment by van Mier [19]; here, the prime stands for inversion of the sign. It was found in the study of Maekawa et al. [28], [29] that the $I_{1e}^{\mathrm{mod'}}/\varepsilon_{c0}'$ - $I_1^{\mathrm{mod'}}/f_c'$ relation up to the critical point is almost linear. On the other hand, we can see from the present results that the relation is nonlinear after the critical point, which implies a dilatancy phenomena in which elastic strains increase after the peak stress.

In **Fig.38(b)**, the $J_{2e}^{\mathrm{mod}}/\varepsilon_{c0}'$ - J_2^{mod}/f_c' relation calculated for the present cyclic compression analysis is compared with that calculated for the experiment by van Mier. The analytical result reflects the experimental result that the peak deviatoric stress value increases and deviatoric damage decreases when the confinement pressure increases.

Fig.38(c) compares the $J_{2e}^{\mathrm{mod}}/\varepsilon_{c0}'$ - K relation calculated for the present analysis with the experiment by van Mier. According to Maekawa et al. [28], the fracture parameter K, representing deviatoric damage under an arbitrary stress condition, depends not only on J_{2e}^{mod} but also on I_{1e}^{mod} and the modified 3rd invariant of elastic deviatoric strain tensor J_{3e}^{mod}.

$$J_{3e}^{\mathrm{mod}} = \sqrt[3]{\frac{1}{3}e_{eij}e_{ejk}e_{eki}} \tag{68}$$

The analytical $J_{2e}^{\mathrm{mod}}/\varepsilon_{c0}'$ - K relation well agrees with the experimental one as well as the one obtained by Maekawa et al., which means that this model predicts degradation of unloading and reloading stiffnesses in the strain-softening regime with accuracy.

In **Fig.38(d)**, the $J_{2e}^{\mathrm{mod}}/\varepsilon_{c0}'$ - $J_{2p}^{\mathrm{mod}}/\varepsilon_{c0}'$ relation calculated for the present cyclic compression analysis is compared with that calculated for the experiment by van Mier. The analytical result follows the trend of the experimental relation, but J_{2p}^{mod} values in the cyclic uniaxial and biaxial compression analyses are underestimated.

Fig.38(e) compares the $J_{2p}^{\mathrm{mod}}/\varepsilon_{c0}'$ - $I_{1p}^{\mathrm{mod}}/\varepsilon_{c0}'$ relation calculated from the results of the present cyclic compression analysis with that calculated for the experiment by van Mier. The present analysis and van Mier's experiment show that $I_{1p}^{\mathrm{mod}}/\varepsilon_{c0}'$ varies from negative values at the initial stage to positive values at the latter stage as $J_{2p}^{\mathrm{mod}}/\varepsilon_{c0}'$ increases. This means that a compressive (negative) volumetric plastic strain is induced up to peak stress due to compaction, while a tensile (positive) volumetric plastic strain is induced after the peak stress due to dilatancy resulting from microcracks and damage under lower confinement pressure.

In the elastoplastic and fracture constitutive model of Maekawa et al. [29], the derivative of the $J_{2p}^{\mathrm{mod}}/\varepsilon_{c0}'$ - $I_{1p}^{\mathrm{mod}}/\varepsilon_{c0}'$ relation is defined as the dilatancy derivative D, which is utilized in formulating the

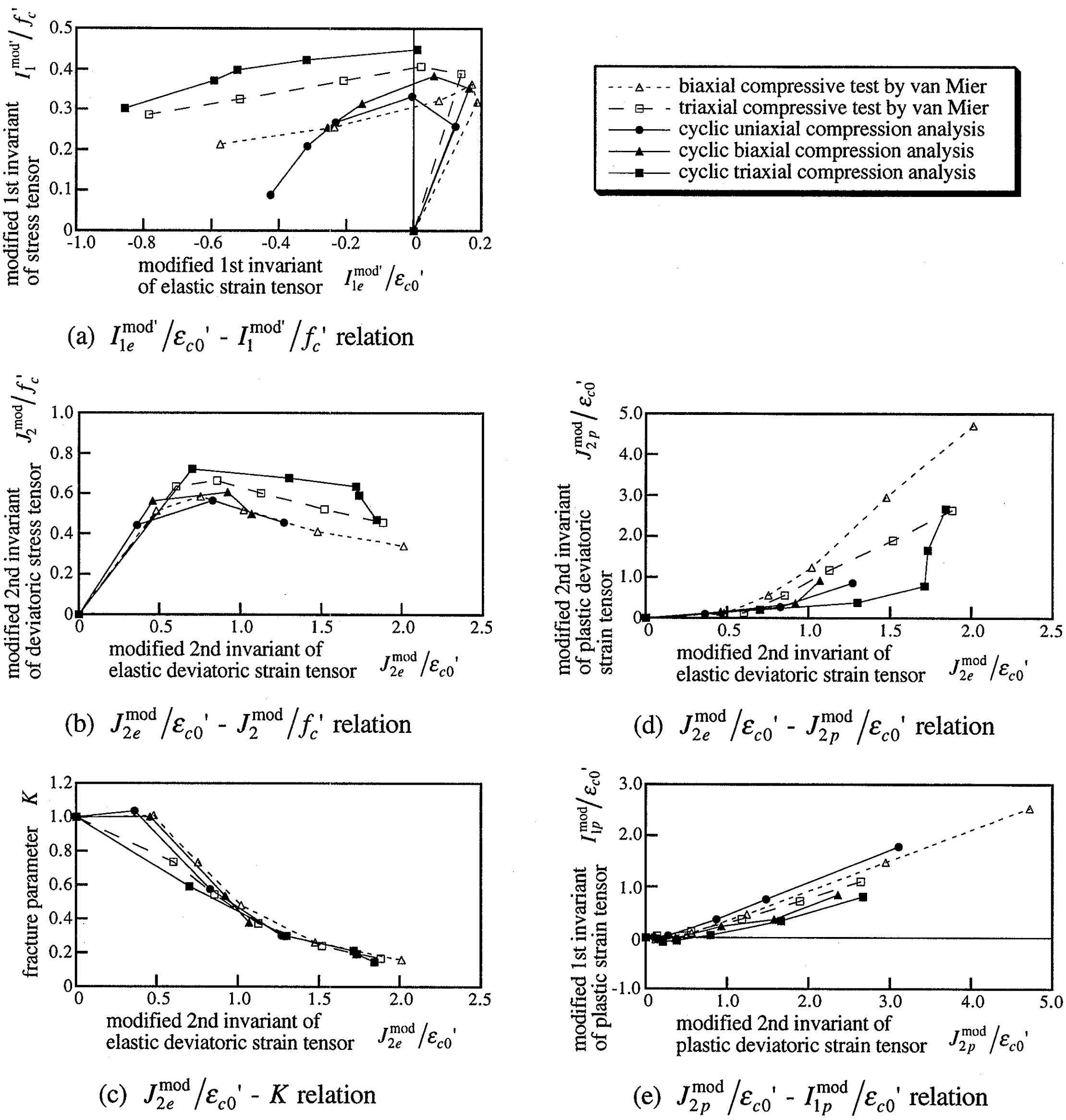

Fig.38 Tensorial invariant relations for Enhanced Microplane Concrete Model

volumetric plasticity associated with shear plasticity.

$$D=\frac{\partial I_{1p}^{\text{mod}}}{\partial J_{2p}^{\text{mod}}} \tag{69}$$

In their study, it was shown that the dilatancy derivative D depends on confinement and damage, and could be formulated as a function of I_{1e}^{mod} and K. In the present calculations, a similar tendency is confirmed: the $J_{2p}^{\text{mod}}/\varepsilon_{c0}'$ - $I_{1p}^{\text{mod}}/\varepsilon_{c0}'$ relation and D depend on confinement pressure and damage.

Although this model is derived without tensorial invariant relations, it has been shown that it can reproduce these relations and predict the cyclic responses of concrete with accuracy.

5. CONCLUSIONS

In this study the difference between the normal-shear and volumetric-deviatoric-shear component formulations, on which the microplane models by Hasegawa and Prat are respectively based, is examined by numerical analysis for a wide range of stress conditions. Then the Hasegawa model (Microplane Concrete Model) is improved to expand its applicability and reformulated as the Enhanced Microplane Concrete Model. This serves as a more general constitutive law. In the last part of the study, the accuracy of the Enhanced Microplane Concrete Model is verified by comparing calculated constitutive relations with experiments reported in the literature. The following conclusions are obtained:

(1) The normal-shear component formulation (Microplane Concrete Model) cannot accurately predict confinement effect and the transition from brittle to ductile fracture, although it has practical accuracy in the case of biaxial and low confinement stress conditions. Since all microplanes ultimately exhibit strain-softening responses in triaxial compression analysis, increases in macroscopic strength and ductility with confinement pressure cannot be predicted well by the normal-shear component formulation.

(2) The prediction accuracy of the volumetric-deviatoric-shear component formulation (Prat model) is poor not only in biaxial and confinement stress conditions, but also in uniaxial tension softening. The calculated total normal responses of microplanes are unacceptable in this model. This means that the microplane, as the basic load-carrying element at a microscopic level, loses its original physical meaning as a result of resolving the normal component into volumetric and deviatoric components.

(3) The previous Microplane Concrete Model is improved to expand its applicability and reformulated as the Enhanced Microplane Concrete Model. One of the major improvements is to take account of the resolved lateral stress in normal compression response on a microplane as well as the resolved lateral strain. Another major improvement is to adopt a model for the transition from brittle to ductile fracture in calculating the shear response on a microplane at increasing resolved normal compression stress. These improvements endow the model with the capability to describe complicated interactions between microplanes through the macroscopic stress tensor. Similar effects are taken into account in the microplane hysteresis rule using the concepts of back-stress and objective-stress.

(4) It is verified that the Enhanced Microplane Concrete Model can accurately predict experimentally obtained constitutive relations for concrete as reported in the literature, covering various stress conditions including uniaxial, biaxial, and triaxial stresses. The model properly predicts confinement effect and the transition from brittle to ductile fracture as well as biaxial failure.

(5) Cyclic behavior under uniaxial, biaxial, and triaxial compression are well described by the Enhanced Microplane Concrete Model. Extracting the invariants of the stress and strain tensors from the analytical responses obtained by this model, the experimental relations of the invariants can be reproduced.

(6) Examination of the microplane responses in each analysis provides an explanation of the load-carrying mechanisms in concrete in terms of responses on the microplanes.

ACKNOWLEDGMENT

This paper is based on the doctoral thesis [7] of the author, who would like to acknowledge the valuable advice given during the course of this study by Professor K. Maekawa of the University of Tokyo and Professor Z. P. Bazant of Northwestern University.

REFERENCES

[1] Bazant, Z. P.: Microplane model for strain-controlled inelastic behaviour, *Mechanics of Engineering Materials*, Chapter 3, Desai, C. S., and Gallagher, R. H., eds., John Wiley & Sons, London, pp.45-59, 1984.

[2] Bazant, Z. P., and Gambarova, P. G.: Crack shear in concrete: Crack band microplane model, *Journal of Structural Engineering, ASCE*, Vol. 110, No. 9, pp.2015-2035, 1984.
[3] Bazant, Z. P., and Prat, P. C.: Microplane model for brittle-plastic material: I. Theory, and II. Verification, *Journal of Engineering Mechanics, ASCE*, Vol. 114, No. 10, pp.1672-1702, 1988.
[4] Ozbolt, J., and Bazant, Z. P.: Microplane model for cyclic triaxial behavior of concrete, *Journal of Engineering Mechanics, ASCE*, Vol. 118, No. 7, pp.1365-1386, 1992.
[5] Carol, I., Bazant, Z. P., and Prat, P. C.: Geometric damage tensor based on microplane model, *Journal of Engineering Mechanics, ASCE*, Vol. 117, No. 10, pp.2429-2448, 1991.
[6] Hasegawa, T., and Bazant, Z. P.: Nonlocal microplane concrete model with rate effect and load cycles. I: General formulation, and II: Application and verification, *Journal of Materials in Civil Engineering, ASCE*, Vol. 5, No. 3, pp.372-410, 1993.
[7] Hasegawa, T.: *Development of the microplane concrete model*, Doctoral thesis, The University of Tokyo, 1994.
[8] Smith, S. S., Willam, K. J., Gerstle, K. H., and Sture, S.: Concrete over the top, or: Is there life after peak?, *ACI Materials Journal*, Vol. 86, No. 5, pp.491-497, 1989.
[9] Bazant, Z. P., and Oh, B. H.: Efficient numerical integration on the surface of a sphere, *Zeitschrift fur Angewandte Mathematik und Mechanik*, Vol. 66, No. 1, pp.37-49, 1986.
[10] Balmer, G. G.: Shearing strength of concrete under high triaxial stress - computation of Mohr's envelope as a curve, *Structural Research Laboratory Report*, United States Department of the Interior, Bureau of Reclamation, No. SP-23, 1949.
[11] Richart, F. E., Brandtzaeg, A., and Brown, R. L.: A study of the failure of concrete under combined compressive stresses, *University of Illinois Engineering Experiment Station Bulletin*, No. 185, 1928.
[12] Kupfer, H., Hilsdorf, H. K., and Rusch, H.: Behavior of concrete under biaxial stresses, *ACI Journal*, Vol. 66, No. 8, pp.656-666, 1969.
[13] Chen, W. F.: *Plasticity in reinforced concrete*, McGraw-Hill Book Company, New York, 1982.
[14] Bazant, Z. P., and Chern, J. C.: Strain softening with creep and exponential algorithm, *Journal of Engineering Mechanics, ASCE*, Vol. 111, No. 3, pp.391-415, 1985.
[15] Bazant, Z. P., and Oh, B. H.: Microplane model for progressive fracture of concrete and rock, *Journal of Engineering Mechanics, ASCE*, Vol. 111, No. 4, pp.559-582, 1985.
[16] Green, S. J., and Swanson, S. R.: Static constitutive relations for concrete, *Report No. AFWL-TR-72-2, Air Force Weapons Laboratory*, Kirtland Air Force Base, 1973.
[17] Yamaguchi, H., Fujimoto, K., and Nomura, S.: Stress-strain relationship for concrete under high triaxial compression: Part 1 Static loading, *Journal of Structural and Construction Engineering (Transactions of AIJ)*, No. 389, pp.99-108, 1988.
[18] Willam, K., Hurlbut, B., and Sture, S.: Experimental and constitutive aspects of concrete failure, *Finite Element Analysis of Reinforced Concrete Structures*, Meyer, C. and Okamura, H., eds., ASCE, New York, pp.226-254, 1986.
[19] van Mier, J. G. M.: *Strain-softening of concrete under multiaxial loading conditions*, Ph.D. thesis, Eindhoven University of Technology, The Netherlands, 1984.
[20] Kosaka, Y., and Tanigawa, Y.: Effect of coarse aggregate on fracture of concrete, (Part 2: Study on microscopic observation), *Transactions of AIJ*, No. 231, pp.1-11, 1975.
[21] Kosaka, Y., Tanigawa, Y., and Oota, F.: Effect of coarse aggregate on fracture of concrete, (Part 1: Model analysis), *Transactions of AIJ*, No. 228, pp.1-11, 1975.
[22] Izumi, M., Mihashi, H., and Sasaki, T.: A study of the concrete fracture mechanism under uniaxial compressive load, *Transactions of AIJ*, No. 289, pp.11-25, 1980.
[23] Krishnaswamy, K. T.: Strength and microcracking of plain concrete under triaxial compression, *ACI Journal*, Vol. 65, No. 10, pp.856-862, 1968.
[24] Niwa, Y., Koyanagi, W., and Nakagawa, K.: Failure processes of concrete under triaxial compressive stress, *Proceedings of JSCE*, No. 185, pp.31-41, 1971.
[25] Ouyang, C., Landis, E., and Shah, S. P.: Damage assessment in concrete using quantitative acoustic emission, *Journal of Engineering Mechanics, ASCE*, Vol. 117, No. 11, pp.2681-2698, 1991.
[26] Buyukozturk, O., Nilson, A. H., and Slate, F. O.: Stress-strain response and fracture of a concrete model in biaxial loading, *ACI Journal*, Vol. 68, No. 8, pp.590-599, 1971.
[27] Liu, T. C. Y., Nilson, A. H., and Slate, F. O.: Stress-strain response and fracture of concrete in uniaxial and biaxial compression, *ACI Journal*, Vol. 69, No. 5, pp.291-295, 1972.
[28] Maekawa, K., Takemura, J., Irawan, P., and Irie, M.: Continuum fracture in concrete nonlinearity under triaxial confinement, *Proceedings of JSCE*, No. 460/V-18, pp.113-122, 1993.

[29] Maekawa, K., Takemura, J., Irawan, P., and Irie, M.: Plasticity in concrete nonlinearity under triaxial confinement, *Proceedings of JSCE*, No. 460/V-18, pp.123-130, 1993.